

MIMO OFDM Dual-Function Radar-Communication Under Error Rate and Beampattern Constraints

Jeremy Johnston, Luca Venturino, *Senior Member, IEEE*, Emanuele Grossi, *Senior Member, IEEE*, Marco Lops, *Fellow, IEEE*, Xiaodong Wang, *Fellow, IEEE*

Abstract—In this work we consider a multiple-input multiple-output (MIMO) dual-function radar-communication (DFRC) system, which senses multiple spatial directions and serves multiple users. Upon resorting to an orthogonal frequency division multiplexing (OFDM) transmission format and a differential phase shift keying (DPSK) modulation, we study the design of the radiated waveforms and of the receive filters employed by the radar and the users. The approach is communication-centric, in the sense that a radar-oriented objective is optimized under constraints on the average transmit power, the power leakage towards specific directions, and the error rate of each user, thus safeguarding the communication quality of service (QoS). We adopt a unified design approach allowing a broad family of radar objectives, including both estimation- and detection-oriented merit functions. We devise a suboptimal solution based on alternating optimization of the involved variables, a convex restriction of the feasible search set, and minorization-maximization, offering a single algorithm for all of the radar merit functions in the considered family. Finally, the performance is inspected through numerical examples.

Index Terms—Dual-function radar-communication, integrated sensing and communication, orthogonal frequency division multiplexing, multiple-input multiple-output, waveform design, filter design, differential phase shift keying.

I. INTRODUCTION

The efficient use of the radio spectrum is a long-standing and challenging problem [1], [2]. Until recently, the frequency bands assigned to different wireless services have been kept mostly separate to avoid co-channel interference and hence simplify the system design; a static frequency planning, however, is inefficient. In the recent past, we have witnessed an increasing demand for mobile communication services that has driven the transition across three standards (3/4/5G) and fostered the proliferation of radar-based services in several areas (for example, industry automation, traffic monitoring, autonomous driving, home surveillance, border patrolling, and

earth monitoring); this has raised the cost for using any bandwidth slice and exacerbated the frequency shortage problem. Several solutions to improve the spectral efficiency have been implemented in communication networks, including the use of sophisticated multiple access schemes and of cognitive radios to allow a more dynamic spectrum management [3]–[5], the coordination of adjacent access points to enable a more aggressive spectrum reuse [6]–[8], and the exploitation of the spatial dimension for data encoding, modulation, and multiplexing [9]–[11]. Important technological advances have been also made in the deployment of radar networks [12], opening up the possibility of simultaneously scheduling multiple functions [13] and implementing cognitive systems which sense the environment, learn relevant information, and then adapt to it [14]; also, the use of multiple-input multiple-output (MIMO) digital transceivers [15] and of the waveform diversity [16] have brought novel degrees of freedom for robust target detection [17], [18], adaptive signal processing [19], [20], and reconfigurable beam-pattern design [21], [22].

Cooperative spectrum sharing among licensed radar and communication systems is a key enabling technology for the efficient exploitation of the available bandwidth. The big divide among the solutions proposed so far is between radar and communication coexistence (RCC), wherein two distinct systems negotiate their transmit/receive strategies to control the mutual interference, and dual-functional radar-communication (DFRC) systems, wherein the radar and communication functions are combined in the same platform [23]–[25]. RCC mainly results in a multi-objective optimization [26]–[30] involving radar- and communication-oriented utilities with separable power constraints; widely-used performance measures are the data rate, the energy efficiency, and the error rate, at the communication side, and the signal-to-interference-plus-noise ratio (SINR), the Cramér Rao bound on the variance of an unbiased estimator of a given unknown parameter, and the mutual information between the received signal and the target response, at the radar side. A DFRC transceiver, conversely, can be implemented by complementing an existing communication module with a full-duplex receiver aimed at detecting the reflections from nearby scatterers [31], [32], in which case enabling the radar function may require the use of sophisticated receive strategies to cope with the imperfect ambiguity function of the communication signal. Alternatively, a message can be embedded into the waveforms radiated by an existing radar: effective strategies are the use of data-

J. Johnston and X. Wang are with the Department of Electrical Engineering, Columbia University, New York, NY 10027, United States (e-mail: j.johnston@columbia.edu; xw2008@columbia.edu).

L. Venturino and E. Grossi are with the Department of Electrical and Information Engineering, University of Cassino and Southern Lazio, 03043 Cassino, Italy, and with CNIT, 43124 Parma, Italy (e-mail: l.venturino@unicas.it; e.grossi@unicas.it).

M. Lops is with the Department of Electrical and Information Technology, University of Naples Federico II, 80138 Naples, Italy, and with CNIT, 43124 Parma, Italy (e-mail: lops@unina.it).

The work of L. Venturino and E. Grossi was supported by the research program “Dipartimenti di Eccellenza 2018–2022” sponsored by the Italian Ministry of Education, University, and Research (MIUR).

dependent coded pulses, the use of frequency/spatial index modulations, and the control of the sidelobes of the transmit beampattern towards the intended destinations [33]–[35].

A. Contribution of the Work

The joint design of the waveforms emitted by the DFRC transmitter and of the radar and communication receivers is a challenging and still debated problem. The goal of this paper is to make a contribution in this domain; in particular, we consider an DFRC system employing an orthogonal frequency division multiplexing (OFDM) transmission format, wherein a MIMO transceiver simultaneously senses the environment and delivers a message to multiple users. Due to its flexibility, OFDM is a good candidate technology to implement a DFRC system [36], [37]; indeed, OFDM is already widely-used in communications [4], while, more recently, has also received extensive attention in radar applications [38].

Previous works on OFDM-DFRC have mainly focused on single-antenna systems where the major degrees of freedom are the power allocation and the user scheduling among the available subcarriers [39], [40] and/or the dynamical assignment of one function (either the radar or the communication) to each subcarrier [41]. The corresponding design strategies have consisted in maximizing the achievable communication sum-rate under a constraint on the radar mutual information [39], minimizing the radiated power under constraints on both the radar and the communication mutual information [40], or maximizing the sum of the radar and the communication mutual information [41]. More recently, a massive MIMO OFDM system has been considered in [42]–[44]. In [42], [43], an access point simultaneously implements a short-range radar and serves multiple downlink users. Its antennas are separated into three groups, which radiate the radar waveforms, receive the echoes from the environment, and radiate the data signals, respectively, and precoding strategies to enhance the system performance are studied. In [44], instead, an access point simultaneously implements a short-range radar and receives signal from multiple uplink users, and the achievable performance are investigated under various operational conditions.

Differently from previous studies, in the present paper we focus on the optimization of a radar-oriented objective function, while safeguarding the communication operation. In particular, the contribution can be summarized as follows.

- Since the MIMO structure expands the number of degrees of freedom, both the transmitter and the receiver can be equipped with space-time filters that control the corresponding beampatterns. Here we tackle the joint design of the DFRC transmitter and of the radar and user receivers and formulate a general resource allocation problem wherein the radar performance is optimized under constraints concerning the average transmit power, the transmit beampattern (so as to limit the power leakage towards specific directions), and the error rate of each user (so as to safeguard the link quality).
- At the radar side, different directions can be inspected on each subcarrier, which allows handling multiple targets. We consider a broad family of merit functions for system

design. This results in a unified design approach, which allows the system engineer to reconfigure the radar task at will and, also, to balance the radar performance on each subcarrier. For example, the considered family includes the *quasi-arithmetic mean* of the radar SINRs on each subcarrier [45]–[47], the weighted-sum of the *mutual information* between the received signal and the target response on each subcarrier [48]–[51], the weighted-sum of the *Fisher information* for the delay estimation on each subcarrier [52], the weighted-sum of the *detection probability* of the likelihood ratio-test on each subcarrier [53], and the weighted-sum of the two *relative entropies* (also known as *Kullback-Leibler divergences*) between the distributions of the received signal under the null hypothesis and its alternative on each subcarrier [54].

- At the communication side, we do not assume full channel state information at the receiver, and a differential phase shift keying (DPSK) modulation is considered: this makes the transmit beampattern independent of the conveyed message and allows the users to employ an incoherent receiver for data demodulation. Needless to say, a coherent modulation scheme could be accounted for if channel state information were available. Also, we include in the model a different statistical characterization of the direct and indirect paths reaching each user.
- Since the considered optimization is not convex, we derive an iterative algorithm—whose structure remains unaltered for all of the radar merit functions in the considered family—to compute a sub-optimal solution, which is based on the alternating optimization of the involved variables, a convex restriction of the feasible search set, and the minorization-maximization algorithm. The proposed procedure monotonically increases the objective function at each iteration and, hence, is convergent.
- Finally, we offer a set of curves showing some achievable radar and communication tradeoffs.

B. Organization and Notation

The remainder of the paper is organized as follows. In Sec. II, the system description is presented. In Sec. III, the proposed resource allocation problem is formulated and discussed, while a suboptimal solution is derived in Sec. IV. In Sec. V, some examples are given to illustrate the achievable tradeoffs between the radar and the communication operation. Concluding remarks are provided in Sec. VI. Finally, the Appendix contains the proofs of some of the presented results.

In the following, \mathbb{R} , \mathbb{R}_+ , and \mathbb{C} are the set of real, non-negative and real, and complex numbers, respectively, while $\bar{\mathbb{R}} = \mathbb{R} \cup \{-\infty, \infty\}$ and $\bar{\mathbb{R}}_+ = \mathbb{R}_+ \cup \{\infty\}$. \mathbb{C}^N and $\mathbb{C}^{N \times N}$ are the set of $N \times 1$ vectors and $N \times N$ matrices with complex entries, respectively; $(\cdot)^*$, $(\cdot)^T$, and $(\cdot)^H$ denote conjugate, transpose and conjugate transpose, respectively; \mathbf{I}_N is the $N \times N$ identity matrix; $\mathbf{1}_N$ and $\mathbf{0}_N$ are the $N \times 1$ vectors with all-one and all-zero entries, respectively. $\text{Tr}\{\mathbf{X}\}$ is the trace of the square matrix \mathbf{X} ; $\lambda_{\min}(\mathbf{X})$ and $\lambda_{\max}(\mathbf{X})$ are the minimum and maximum eigenvalue of the Hermitian matrix \mathbf{X} , respectively. $\text{vec}\{\mathbf{X}\}$ is the vector obtained by stacking

up the columns of \mathbf{X} . $\mathbf{X} \succeq 0$ and $\mathbf{X} \preceq 0$ means that \mathbf{X} is Hermitian positive and negative semidefinite, respectively; if \mathbf{X}_1 and \mathbf{X}_2 are Hermitian matrices, then $\mathbf{X}_1 \succeq \mathbf{X}_2$ means that $\mathbf{X}_1 - \mathbf{X}_2 \succeq 0$. $\text{diag}(\{x_n\})$ is the diagonal matrix with entries x_1, \dots, x_N on the main diagonal. We interchangeably use $f(x_1, \dots, x_N)$, $f(\mathbf{x})$, and $f(\{x_n\})$ to denote a function f of $\mathbf{x} = (x_1, \dots, x_N)^\top$. f' , f'' , and f''' are the first, second, and third derivative of f , respectively. C^k denotes the differentiability class of order k . f^{-1} , ∇_f and ∇_f^2 are the inverse function, the gradient and the Hessian of f , respectively. $\mathbb{1}_{\mathcal{A}}$ is the indicator function of the condition \mathcal{A} , i.e., $\mathbb{1}_{\mathcal{A}} = 1$, if \mathcal{A} holds true, and $\mathbb{1}_{\mathcal{A}} = 0$, otherwise in the notation paragraph. Finally, \otimes and \mathbf{j} indicate the Kronecker product and the imaginary unit, respectively.

II. SYSTEM DESCRIPTION

We consider an OFDM wireless system consisting of a DFRC transmitter, a co-located radar receiver, and M communication users, each equipped with a linear array with closely-spaced antennas.¹ We denote by N_t , N_r , and N_m the number of antennas at the transmitter, the radar receiver, and the m -th user, respectively. The OFDM symbol duration is much longer than the maximum propagation delay, so that a narrowband assumption holds on each subcarrier [36], [38]. A subset of K subcarriers is employed to simultaneously implement the radar and communication functions, while the other ones are not considered in this work. On each shared subcarrier, the transmitter aims to illuminate the direction of a prospective target while broadcasting a message to the users. We resort here to a DPSK modulation [4] for data transmission; this is motivated by the facts that an incoherent receiver can be employed by each user and that the resulting transmit beampattern is independent of the selected data symbol.

A. Communication Side

A direct path and/or $Q_m \geq 0$ indirect paths (produced by as many far-field independent scatterers) can be present between the transmitter and the m -th user. Accordingly, its discrete-time received signal on the k -th subcarrier is modeled as

$$y_{k,m} = d_k \left(\underbrace{\beta_{k,m,0} \text{Tr}\{\mathbf{W}_{k,m}^H \mathbf{g}_{k,m}(\bar{\phi}_{m,0}) \mathbf{s}_k^\top(\phi_{m,0}) \mathbf{U}_k\}}_{\text{direct link}} + \underbrace{\sum_{q=1}^{Q_m} \beta_{k,m,q} \text{Tr}\{\mathbf{W}_{k,m}^H \mathbf{g}_{k,m}(\bar{\phi}_{m,q}) \mathbf{s}_k^\top(\phi_{m,q}) \mathbf{U}_k\}}_{\text{indirect links}} \right) + \text{Tr}\{\mathbf{W}_{k,m}^H \mathbf{Z}_{k,m}\} \quad (1)$$

where: $\beta_{k,m,0} \in \mathbb{C}$ is the response of the direct path, while $\bar{\phi}_{m,0}$ and $\phi_{m,0}$ are the corresponding angles of arrival and departure, respectively;² $\beta_{k,m,q} \in \mathbb{C}$, for $q = 1, \dots, Q_m$, is the response of the q -th indirect path, while $\bar{\phi}_{m,q}$ and $\phi_{m,q}$ are the corresponding angles of arrival and departure, respectively; $\mathbf{g}_{k,m}(\bar{\varphi}) \in \mathbb{C}^{N_m}$ and $\mathbf{s}_k(\varphi) \in \mathbb{C}^{N_t}$ are the

receive and transmit steering vectors, respectively, which are normalized to have entries with unit magnitude; for example, if a uniform receive array is employed, we have $\mathbf{g}_{k,m}(\bar{\varphi}) = (1 e^{-j2\pi \frac{f_k b_m}{c} \sin(\bar{\varphi})} \dots e^{-j2\pi \frac{f_k b_m}{c} \sin(\bar{\varphi})(N_m-1)})^\top$, where f_k is the center frequency of the k -th subcarrier, b_m is the element spacing, and c is the speed of light; $\mathbf{U}_k \in \mathbb{C}^{N_t \times T}$ is the code matrix employed by the transmitter, which spans T OFDM symbols; $\mathbf{W}_{k,m} \in \mathbb{C}^{N_m \times T}$ is the filter employed by the user; $d_k \in \mathcal{D} = \{1, e^{j2\pi/D}, \dots, e^{j2\pi(D-1)/D}\}$ is the DPSK symbol to be broadcast, with D being the cardinality of the constellation \mathcal{D} ; and $\mathbf{Z}_{k,m} \in \mathbb{C}^{N_m \times T}$ is the disturbance vector.

We assume that $\beta_{k,m,0}$ has a random phase, while its magnitude is deterministic and tied to the pathloss; $|\beta_{k,m,0}| = 0$ if no direct link is present, while $|\beta_{k,m,0}| > 0$ otherwise. Also, we consider a Swerling I fluctuation model in each indirect path (as it includes the radar cross-section of the reflecting object), whereby $\beta_{k,m,q}$ is modeled as a circularly-symmetric Gaussian random variable with variance $\sigma_{\beta,k,m,q}^2 > 0$ [55]. Finally, we model the entries of $\mathbf{Z}_{k,m}$ as independent circularly-symmetric Gaussian random variables with variance $\sigma_{z,k,m}^2 > 0$.

Upon defining $\mathbf{u}_k = \text{vec}\{\mathbf{U}_k\}$, $\mathbf{w}_{k,m} = \text{vec}\{\mathbf{W}_{k,m}\}$, $\mathbf{z}_{k,m} = \text{vec}\{\mathbf{Z}_{k,m}\}$, and $\mathbf{G}_{k,m}(\bar{\varphi}, \varphi) = \mathbf{I}_T \otimes \mathbf{g}_{k,m}(\bar{\varphi}) \mathbf{s}_k^\top(\varphi)$, the signal in (1) can be recast as

$$y_{k,m} = d_k h_{k,m} + \mathbf{w}_{k,m}^H \mathbf{z}_{k,m} \quad (2)$$

where $h_{k,m} = \sum_{q=0}^{Q_m} \beta_{k,m,q} \mathbf{w}_{k,m}^H \mathbf{G}_{k,m}(\bar{\phi}_{m,q}, \phi_{m,q}) \mathbf{u}_k$ is the channel response resulting from the superposition of the all paths reaching user m on subcarrier k . Notice that $h_{k,m}$ is a complex random variable, and its magnitude follows a Rice distribution whose scale and shape parameters are [4]

$$\nu_{k,m} = |\beta_{k,m,0}|^2 |\mathbf{w}_{k,m}^H \mathbf{G}_{k,m}(\bar{\phi}_{m,0}, \phi_{m,0}) \mathbf{u}_k|^2 + \sum_{q=1}^{Q_m} \sigma_{\beta,k,m,q}^2 |\mathbf{w}_{k,m}^H \mathbf{G}_{k,m}(\bar{\phi}_{m,q}, \phi_{m,q}) \mathbf{u}_k|^2 \quad (3a)$$

$$\kappa_{k,m} = \frac{|\beta_{k,m,0}|^2 |\mathbf{w}_{k,m}^H \mathbf{G}_{k,m}(\bar{\phi}_{m,0}, \phi_{m,0}) \mathbf{u}_k|^2}{\sum_{q=1}^{Q_m} \sigma_{\beta,k,m,q}^2 |\mathbf{w}_{k,m}^H \mathbf{G}_{k,m}(\bar{\phi}_{m,q}, \phi_{m,q}) \mathbf{u}_k|^2} \quad (3b)$$

respectively. The parameter $\nu_{k,m} > 0$ is the power received from all paths, while $\kappa_{k,m} \geq 0$ provides the ratio of the power along the direct path to that along the indirect paths.

Assuming that $h_{k,m}$ remains constant over two transmissions, we adopt an incoherent receiver to detect the phase offset over consecutive data symbols [4]. We underline that such a receiver does not require the knowledge of $h_{k,m}$ for data demodulation. For $D = 2$, the error probability for the m -th user on the k -th subcarrier is [56]

$$E_{k,m} = \frac{1 + \kappa_{k,m}}{2(1 + \kappa_{k,m} + \text{SNR}_{k,m})} \exp\left\{ \frac{-\kappa_{k,m} \text{SNR}_{k,m}}{\kappa_{k,m} + \text{SNR}_{k,m}} \right\} \quad (4)$$

where

$$\text{SNR}_{k,m} = \frac{\nu_{k,m}}{\sigma_{z,k,m}^2 \|\mathbf{w}_{k,m}\|^2} \quad (5)$$

is the signal-to-noise-ratio (SNR). Notice that $E_{k,m}$ in (4) is decreasing with both $\kappa_{k,m}$ and $\text{SNR}_{k,m}$ (see also [56, Fig. 1]). For $D > 2$, an integral expression of the error probability $E_{k,m}$ is found in [57, Eq. (5)] and omitted here for brevity; while

¹The following developments can be also extended to planar arrays.

²Hereafter, all angles of arrival/departure are measured with respect to the array broadside direction and are positive when moving clockwise.

this expression is more cumbersome, it still shows that $E_{k,m}$ is decreasing with both $\kappa_{k,m}$ and $\text{SNR}_{k,m}$.

B. Radar Side

The radar inspects the direction ψ_k on subcarrier k and is aware of the presence of the self-interference (clutter) produced by $J \geq 0$ independent scatterers located in the directions $\theta_1, \dots, \theta_J$, with $\theta_j \neq \psi_k$ for any j and k . Accordingly, the discrete-time signal received on the k -th subcarrier is modeled as

$$y_k = \underbrace{d_k \eta_k \text{Tr}\{\mathbf{W}_k^H \mathbf{g}_k(\psi_k) \mathbf{s}_k^T(\psi_k) \mathbf{U}_k\}}_{\text{target}} + \underbrace{d_k \sum_{j=1}^J \alpha_{k,j} \text{Tr}\{\mathbf{W}_k^H \mathbf{g}_k(\theta_j) \mathbf{s}_k^T(\theta_j) \mathbf{U}_k\}}_{\text{clutter}} + \text{Tr}\{\mathbf{W}_k^H \mathbf{Z}_k\} \quad (6)$$

where $\eta_k \in \mathbb{C}$ is the response of the target, $\alpha_{k,j} \in \mathbb{C}$ is the response of the j -th scatterer, $\mathbf{g}_k(\varphi) \in \mathbb{C}^{N_r}$ is the receive steering vector, $\mathbf{W}_k \in \mathbb{C}^{N_r \times T}$ is the filter employed by the radar receiver, and $\mathbf{Z}_k \in \mathbb{C}^{N_r \times T}$ is the disturbance vector.³ We assume a Swerling I fluctuation for both the target and the clutter, whereby η_k and $\alpha_{k,j}$ are independent circularly-symmetric Gaussian variables with variance $\sigma_{\eta,k}^2 > 0$ and $\sigma_{\alpha,k,j}^2 > 0$, respectively [55]; accordingly, the unit-magnitude data symbol d_k can be absorbed into η_k and $\alpha_{k,j}$ and does not play any role in the implementation of the radar receiver. Also, the entries of \mathbf{Z}_k are modeled as independent circularly-symmetric Gaussian variables with variance $\sigma_{z,k}^2 > 0$.

Letting $\mathbf{w}_k = \text{vec}\{\mathbf{W}_k\}$, $\mathbf{z}_k = \text{vec}\{\mathbf{Z}_k\}$, and $\mathbf{G}_k(\theta_j) = \mathbf{I}_T \otimes \mathbf{g}_k(\theta_j) \mathbf{s}_k^T(\theta_j)$, the received signal can be rewritten as

$$y_k = \eta_k \mathbf{w}_k^H \mathbf{G}_k(\psi_k) \mathbf{u}_k + \sum_{j=1}^J \alpha_{k,j} \mathbf{w}_k^H \mathbf{G}_k(\theta_j) \mathbf{u}_k + \mathbf{w}_k^H \mathbf{z}_k \quad (7)$$

and the corresponding SINR is

$$\text{SINR}_k = \frac{\sigma_{\eta,k}^2 |\mathbf{w}_k^H \mathbf{G}_k(\psi_k) \mathbf{u}_k|^2}{\sum_{j=1}^J \sigma_{\alpha,k,j}^2 |\mathbf{w}_k^H \mathbf{G}_k(\theta_j) \mathbf{u}_k|^2 + \sigma_{z,k}^2 \|\mathbf{w}_k\|^2} \quad (8)$$

for $k = 1, \dots, K$. We now consider the following family of merit functions for system design

$$f(\text{SINR}_1, \dots, \text{SINR}_K) \quad (9)$$

where $f: \mathbb{R}_+^K \rightarrow \mathbb{R}_+$ is any increasing function that is either concave or minorized⁴ at any point $\mathbf{x}_0 \in \mathbb{R}_+^K$ by a concave function $\zeta(\cdot | \mathbf{x}_0)$. Meaningful examples of radar merit functions will be provided later in Sec. III-A.

The following remarks are now in order. The radar pointing direction on each subcarrier can be that of a communication user or of another (prospective) object; likewise, the clutter

³Notice here that we use the same letter y to denote the signal received by both the user m and the radar. The understating is that the first subscript indexes the k -th subcarrier, while the second subscript, if present, identifies the m -th user, and, if absent, the radar receiver. A similar choice is made to denote the receive steering vector, the additive noise, and the receive filter.

⁴The function $\zeta(\cdot | \mathbf{x}_0)$ minorizes f at \mathbf{x}_0 if $f(\mathbf{x}) \geq \zeta(\mathbf{x} | \mathbf{x}_0)$, $\forall \mathbf{x}$, and $f(\mathbf{x}_0) = \zeta(\mathbf{x}_0 | \mathbf{x}_0)$ [58].

may be caused by nearby users or other objects. The radar may inspect different directions on different subcarriers, thus handling multiple targets. Interestingly enough, the above model and the following design methodology can be also extended to the case where the radar simultaneously inspects multiple directions on the same subcarrier employing as many receive filters: in this case, the family of merit functions in (9) is modified to account for the individual SINR's on all inspected directions across all subcarriers; to keep the exposition concealed this generalization has been omitted.

C. Transmit Beampattern

The power radiated by the DFRC transmitter towards ξ on subcarrier k can be written as

$$\Delta_k(\mathbf{u}_k, \xi) = \frac{1}{T} \|\mathbf{s}_k^T(\xi) \mathbf{U}_k\|^2 = \frac{1}{T} \mathbf{u}_k^H (\mathbf{I}_T \otimes \mathbf{s}_k^*(\xi) \mathbf{s}_k^T(\xi)) \mathbf{u}_k. \quad (10)$$

Notice that $\Delta_k(\mathbf{u}_k, \xi) \leq N_t \mathcal{P}$, where \mathcal{P} is the available power, with equality when all the power is assigned to subcarrier k (i.e., $\mathbf{u}_p = \mathbf{0}_{N_t}$ for $p \neq k$ and $\|\mathbf{u}_k\|^2/T = \mathcal{P}$) and $\mathbf{u}_k \propto \mathbf{1}_T \otimes \mathbf{s}_k^*(\xi)$. It is desirable that the transmit beampattern in each subcarrier illuminate the directions corresponding to the prospective target and the connected users, while reducing the power leakage elsewhere, so as to limit the interference possibly caused to the radar receiver and to other co-channel systems operating nearby. We denote by $\xi_{k,1}, \dots, \xi_{k,L_k}$ the directions to be protected on subcarrier k , with $\xi_{k,\ell} \neq \psi_k$.

III. PROBLEM FORMULATION

We assume here cognition of the surrounding environment, i.e., that the parameters $\{\bar{\phi}_{m,q}, \phi_{m,q}\}$, $\{|\beta_{k,m,0}|\}$, $\{\sigma_{\beta,k,m,q}^2\}$, $\{\sigma_{z,k,m}^2\}$, $\{\theta_j\}$, $\{\sigma_{\alpha,k,j}^2\}$, and $\{\sigma_{z,k}^2\}$ can be estimated [14], [24]; on the other hand, the target powers $\{\sigma_{\eta,k}^2\}$ may be set to a nominal value, as usual in radar design.

For a given \mathcal{P} , we aim at maximizing a radar merit function of the form in (9), while guaranteeing a desired error rate for each user and constraining the transmit beampattern towards specific directions. The design variables are the transmit code $\{\mathbf{u}_k\}$, which allocate the power across the subcarriers and shape the transmit beampattern, and the receiver filters $\{\mathbf{w}_k, \mathbf{w}_{k,m}\}$, which provide additional degrees of freedom for interference management. The problem to be solved is

$$\begin{aligned} & \max_{\{\mathbf{u}_k, \mathbf{w}_k, \mathbf{w}_{k,m}\}} f(\{\text{SINR}_k(\mathbf{u}_k, \mathbf{w}_k)\}) \\ & \text{s.t. C1: } \frac{1}{T} \sum_{k=1}^K \|\mathbf{u}_k\|^2 \leq \mathcal{P} \\ & \text{C2: } \Delta_k(\mathbf{u}_k, \xi_{k,\ell}) \leq \delta_{k,\ell} N_t \mathcal{P}, \quad \forall k, \ell \\ & \text{C3: } E_{k,m}(\mathbf{u}_k, \mathbf{w}_{k,m}) \leq \epsilon_{k,m}, \quad \forall k, m \end{aligned} \quad (11)$$

where $\delta_{k,\ell} \in [0, 1]$ and $\epsilon_{k,m} \in (0, 1/2)$. The above formulation can be readily modified to serve a different set of users on each subcarrier. For example, if user m only needs to receive the message sent on the first subcarrier, then the constraints on the error probability in the other subcarriers are simply removed; thus an orthogonal frequency division multiple access (OFDMA) can be obtained as a special case.

Problem (11) is non-convex and hence difficult to solve. In the remaining part of this section we provide more insights into Problem (11); then in Section IV we propose a procedure to compute a suboptimal solution.

A. Examples of Radar Merit Functions

The family reported in (9) encompasses several relevant merit functions. For example, we can consider the p -th power mean, with $p \leq 1$, of the SINRs on each subcarrier [45]–[47]; in this case we have⁵

$$f(\mathbf{x}) = \left(\sum_{k=1}^K \mu_k x_k^p \right)^{1/p} \quad (12)$$

where $\{\mu_k\}$ are positive weights with $\sum_{k=1}^K \mu_k = 1$, which can be employed to give different priorities to different subcarriers. The function in (12) is increasing and its concavity follows from the Minkowski's inequality [46][Ch. 4, Th. 9]. Also, its value gets more biased towards its smallest argument as p is decreased; in particular, it reduces to the arithmetic mean for $p = 1$, the geometric mean for $p \rightarrow 0$, the harmonic mean for $p = -1$, and $\min_{k \in \{1, \dots, K\}} x_k$ for $p \rightarrow -\infty$.

We can also consider the *quasi-arithmetic mean* (also known as *generalized mean*) of the SINRs generated by a continuous strictly monotone function $\gamma: \bar{\mathbb{R}}_+ \rightarrow \bar{\mathbb{R}}$ [45], [46], so that

$$f(\mathbf{x}) = \gamma^{-1} \left(\sum_{k=1}^K \mu_k \gamma(x_k) \right). \quad (13)$$

This function is increasing and subsumes the p -th power mean for $\gamma(x) = x^p$ and the Geometric mean for $\gamma(x) = \ln x$; in the other cases, we can prove its concavity by exploiting the following proposition,⁶ whose proof is provided in Appendix A.

Proposition 1. *Let $\gamma: \bar{\mathbb{R}}_+ \rightarrow \bar{\mathbb{R}}$ be a C^4 function that is either strictly increasing and strictly concave or strictly decreasing and strictly convex. Then $f(\mathbf{x}) = \gamma^{-1}(\sum_{k=1}^K \mu_k \gamma(x_k))$ is concave if and only if γ'/γ'' is convex.*

For example, $\gamma(x) = a^x$, with $a \in (0, 1)$, satisfies the conditions of Proposition 1, so that the resulting *exponential mean* [46], [59] $f(\mathbf{x}) = \log_a(\sum_{k=1}^K \mu_k a^{x_k})$ is concave. Also, $\gamma(x) = a^{1/x}$, with $a > 1$, satisfies the conditions of Proposition 1, so that the resulting *radical mean* [46] $f(\mathbf{x}) = (\log_a(\sum_{k=1}^K \mu_k a^{1/x_k}))^{-1}$ is concave.

Furthermore, we can consider the weighted sum of the *mutual information* between the received signal and the target response on each subcarrier, that is relevant in target classification. In this case, we have [48]–[51]

$$f(\mathbf{x}) = \sum_{k=1}^K \mu_k \ln(1 + x_k) \quad (14)$$

which is increasing and concave.

Additionally, we can consider the weighted-sum of the *Fisher information* for the delay estimation on each subcarrier,

⁵We adopt the convention that $\frac{1}{0} = \infty$, $\frac{1}{\infty} = 0$, and $\alpha + \infty = \infty$ for any $\alpha \geq 0$; accordingly, for $p < 0$, $f(\mathbf{x}) = 0$ if $x_k = 0$ for any $k \in \{1, \dots, K\}$.

⁶The result of this proposition still holds when the domain of γ is a closed interval $[a, b] \subseteq \bar{\mathbb{R}}$, and the domain of f is changed accordingly.

which is related to the accuracy in target ranging. In this case, up to an irrelevant scaling factor, we have [52, cfr. Eq. (35)]

$$f(\mathbf{x}) = \sum_{k=1}^K \frac{\mu_k x_k^2}{1 + x_k} \quad (15)$$

which is an increasing function. Moreover, since each term of the summation is convex and, therefore, lower-bounded by the tangent line, we have that f is minorized at any \mathbf{x}_0 by the following concave (in fact, linear) function

$$\zeta(\mathbf{x}|\mathbf{x}_0) = \sum_{k=1}^K \mu_k \left(\frac{x_{0,k}^2}{1 + x_{0,k}} + \frac{2x_{0,k} + x_{0,k}^2}{(1 + x_{0,k})^2} (x_k - x_{0,k}) \right). \quad (16)$$

Moreover, we can consider the weighted sum of the detection probability of the likelihood ratio-test on each subcarrier. In this case, we have [53]

$$f(\mathbf{x}) = \sum_{k=1}^K \mu_k P_{\text{fa},k}^{1/(1+x_k)} \quad (17)$$

where $P_{\text{fa},k}$ is the probability of false alarm on the k -th subcarrier. This function is increasing, and, since

$$\left(P_{\text{fa},k}^{1/(1+x_k)} \right)' = - \frac{P_{\text{fa},k}^{1/(1+x_k)} \ln P_{\text{fa},k}}{(1 + x_k)^2} \quad (18a)$$

$$\begin{aligned} \left(P_{\text{fa},k}^{1/(1+x_k)} \right)'' &= P_{\text{fa},k}^{1/(1+x_k)} \left(\frac{(\ln P_{\text{fa},k})^2}{(1 + x_k)^4} + \frac{2 \ln P_{\text{fa},k}}{(1 + x_k)^3} \right) \\ &\geq - \frac{(\sqrt{3} - 3)^4 e^{\sqrt{3}-3}}{\sqrt{3} (\ln P_{\text{fa},k})^2} \end{aligned} \quad (18b)$$

a quadratic lower-bound for each term of the summation is readily obtained through Taylor's theorem. Therefore, f is minorized at any \mathbf{x}_0 by the following concave function

$$\begin{aligned} \zeta(\mathbf{x}|\mathbf{x}_0) &= \sum_{k=1}^K \mu_k \left(P_{\text{fa},k}^{1/(1+x_{0,k})} - \frac{P_{\text{fa},k}^{1/(1+x_{0,k})} \ln P_{\text{fa},k}}{(1 + x_{0,k})^2} \right. \\ &\quad \left. \times (x_k - x_{0,k}) - \frac{(\sqrt{3} - 3)^4 e^{\sqrt{3}-3}}{2\sqrt{3} (\ln P_{\text{fa},k})^2} (x_k - x_{0,k})^2 \right). \end{aligned} \quad (19)$$

Finally, denote by \mathcal{H}_0 and \mathcal{H}_1 the null hypothesis (i.e., no target is present) and its alternative, respectively. We can consider the weighted-sum of the two *relative entropies* between \mathcal{H}_0 and \mathcal{H}_1 and between \mathcal{H}_1 and \mathcal{H}_0 on each subcarrier, that can be used to control the average number of samples needed to make a decision in a sequential probability ratio test with given probabilities of detection and false alarm. In this case, we have [54, cfr. Sec. III]

$$f(\mathbf{x}) = \sum_{k=1}^K \mu_k f_k(x_k) \quad (20)$$

where $f_k(x_k) = (1 - 2\omega_k) \ln(1 + x_k) + x_k \frac{\omega_k x_k - (1 - 2\omega_k)}{1 + x_k}$, with $\omega_k \in [0, 1]$. This function is increasing, and, since

$$f_k'(x_k) = \frac{x_k(1 + \omega_k x_k)}{(1 + x_k)^2} \quad (21a)$$

$$f_k''(x_k) = \frac{1 - (1 - 2\omega_k)x_k}{(1 + x_k)^3} \geq - \frac{(1 - 2\omega_k)^3}{27(1 - \omega_k)^2} \quad (21b)$$

each term of the summation is convex, if $\omega_k \geq 1/2$. Therefore, f is minorized at any \mathbf{x}_0 by the following concave function

$$\zeta(\mathbf{x}|\mathbf{x}_0) = \sum_{k=1}^K \mu_k \left(f_k(x_{0,k}) + f'_k(x_{0,k})(x_k - x_{0,k}) - \frac{(1 - 2\omega_k)^3}{54(1 - \omega_k)^2} (x_k - x_{0,k})^2 \mathbb{1}_{\{\omega_k < 1/2\}} \right). \quad (22)$$

B. Handling the Error Probability Constraint

Varying \mathbf{u}_k and/or $\mathbf{w}_{k,m}$ may have opposite effects on $\kappa_{k,m}$ and $\nu_{k,m}$ in (3); accordingly, the best tradeoff in terms of the error probability is in general not simple to assess. Interestingly, the dependency of $E_{k,m}$ upon \mathbf{u}_k and $\mathbf{w}_{k,m}$ simplifies when $\kappa_{k,m} = \infty$ and $\kappa_{k,m} = 0$, as discussed next.

If $\kappa_{k,m} = \infty$, then only a direct path is present and no signal fading is observed; in this case, we have

$$E_{k,m} = \frac{1}{2} e^{-\text{SNR}_{k,m}^d} \quad (23)$$

for $D = 2$, and⁷

$$E_{k,m} \approx 2Q \left(\sqrt{\text{SNR}_{k,m}^d \sin^2 \frac{\pi}{D}} \right) \quad (24)$$

for $D > 2$ and $\text{SNR}_{k,m}^d \gg 1$, where $Q(x) = \frac{1}{\sqrt{2\pi}} \int_x^\infty e^{-t^2/2} dt$ and

$$\text{SNR}_{k,m}^d = \frac{|\beta_{k,m,0}|^2 |\mathbf{w}_{k,m}^H \mathbf{G}_{k,m}(\bar{\phi}_{m,0}, \phi_{m,0}) \mathbf{u}_k|^2}{\sigma_{z,k,m}^2 \|\mathbf{w}_{k,m}\|^2}. \quad (25)$$

If $\kappa_{k,m} = 0$, then only the indirect paths are present and Rayleigh fading is observed; in this case, we have

$$E_{k,m} = \frac{1}{2(1 + \text{SNR}_{k,m}^i)} \quad (26)$$

for $D = 2$, and [60]

$$E_{k,m} \leq \frac{2\pi - \frac{2\pi}{D} + \sin \frac{2\pi}{D}}{2\pi \text{SNR}_{k,m}^i \sin^2 \frac{\pi}{D}} \quad (27)$$

for $D > 2$, where

$$\text{SNR}_{k,m}^i = \frac{\sum_{q=1}^{Q_m} \sigma_{\beta,k,m,q}^2 |\mathbf{w}_{k,m}^H \mathbf{G}_{k,m}(\bar{\phi}_{m,q}, \phi_{m,q}) \mathbf{u}_k|^2}{\sigma_{z,k,m}^2 \|\mathbf{w}_{k,m}\|^2}. \quad (28)$$

For any \mathbf{u}_k and $\mathbf{w}_{k,m}$, $\kappa_{k,m} = \infty$ if the transmitter and user m are in the line of sight and no close scatterers are present, while $\kappa_{k,m} = 0$ if an obstacle blocks the direct path and nearby scatterers redirect the signal emitted by the transmitter towards user m . In all other cases, we can sub-optimally force $\kappa_{k,m}$ to be either ∞ or 0 by operating on the receive filter $\mathbf{w}_{k,m}$, assuming that sufficient degrees of freedom are available. To be more specific, $\kappa_{k,m}$ can be set equal to infinity by choosing $\mathbf{w}_{k,m}$ in the null space of the matrices $\{\mathbf{G}_{k,m}^H(\bar{\phi}_{m,q}, \phi_{m,q})\}_{q=1}^{Q_m}$, so as to zero-force the indirect signals: this is possible if the number of receive

antennas is greater than the number of indirect paths (i.e., $N_m > Q_m$). Similarly, $\kappa_{k,m}$ can be set equal to zero by choosing $\mathbf{w}_{k,m}$ in the null space of $\mathbf{G}_{k,m}^H(\bar{\phi}_{m,0}, \phi_{m,0})$, so as to zero-force the direct signal: this is possible if the user has two or more antennas. Clearly, forcing $\kappa_{k,m} \in \{0, \infty\}$ amounts to adding a constraint into the optimization problem, that may lead to a sub-optimum solution.

If $\kappa_{k,m} \in \{\infty, 0\}$, it is verified from (23)–(28) that upper bounding $E_{k,m}$ amounts to lower bounding

$$\text{SNR}_{k,m} = \begin{cases} \text{SNR}_{k,m}^d, & \text{if } \kappa_{k,m} = \infty \\ \text{SNR}_{k,m}^i, & \text{if } \kappa_{k,m} = 0. \end{cases} \quad (29)$$

Hence, the problem to be solved becomes

$$\begin{aligned} & \max_{\{\mathbf{u}_k, \mathbf{w}_k, \mathbf{w}_{k,m}\}} f(\{\text{SINR}_k(\mathbf{u}_k, \mathbf{w}_k)\}) \\ \text{s.t. C1: } & \frac{1}{T} \sum_{k=1}^K \|\mathbf{u}_k\|^2 \leq \mathcal{P} \\ \text{C2: } & \Delta_k(\mathbf{u}_k, \xi_{k,\ell}) \leq \delta_{k,\ell} N_t \mathcal{P}, \forall k, \ell \\ \text{C3: } & \text{SNR}_{k,m}(\mathbf{u}_k, \mathbf{w}_{k,m}) \geq \rho_{k,m}, \forall m, k \\ \text{C4: } & \mathbf{w}_{k,m} \in \mathcal{W}_{k,m} \end{aligned} \quad (30)$$

where

$$\rho_{k,m} = \begin{cases} \rho_{k,m}^d, & \text{if } \kappa_{k,m} = \infty \\ \rho_{k,m}^i, & \text{if } \kappa_{k,m} = 0 \end{cases} \quad (31)$$

is the minimum SNR required to satisfy the error rate constraint for the user m on subcarrier k and $\mathcal{W}_{k,m} = \{\mathbf{w}_{k,m} \in \mathbb{C}^{TN_m} : \kappa_{k,m} \in \{\infty, 0\}\}$.

Since the feasible search set of Problem (30) is included in that of Problem (11), we have the following result.

Proposition 2. *The solution to Problem (30) provides a lower bound to the solution to Problem (11).*

IV. PROPOSED ALGORITHM

We compute here a suboptimal solution to (30) by resorting to an alternating maximization. Starting from a feasible point, the objective function is maximized with respect to each of the block variables $\{\mathbf{u}_k\}$, $\{\mathbf{w}_k\}$, and $\{\mathbf{w}_{k,m}\}$, taken in a cyclic order, while keeping the other ones fixed at their previous values. In the following, we discuss in detail the update of each block variable and the selection of the starting point. The overall procedure is summarized in Algorithm 1 and is monotonically convergent, as the value of the objective function is not decreased at each iteration. We underline here that convergence to a local/global optimum solution is not guaranteed as not all sub-problems are optimally solved.

A. Update of the Transmit Code

Upon defining $\Psi_{k,1} = \sigma_{\eta,k}^2 \mathbf{G}_k^H(\psi_k) \mathbf{w}_k \mathbf{w}_k^H \mathbf{G}_k(\psi_k)$ and $\Psi_{k,2} = \sum_{j=1}^J \sigma_{\alpha,k,j}^2 \mathbf{G}_k^H(\theta_j) \mathbf{w}_k \mathbf{w}_k^H \mathbf{G}_k(\theta_j)$, the problem to be solved is

$$\max_{\{\mathbf{u}_k\}} f \left(\left\{ \frac{\mathbf{u}_k^H \Psi_{k,1} \mathbf{u}_k}{\mathbf{u}_k^H \Psi_{k,2} \mathbf{u}_k + \sigma_{z,k}^2 \|\mathbf{w}_k\|^2} \right\} \right), \quad \text{s.t. C1, C2, C3} \quad (32)$$

⁷DPSK loses about 3 dB with respect to the coherent PSK at large SNR's, and, in this regime, the nearest neighbor approximation to the error probability of the coherent PSK is tight.

Algorithm 1 Proposed sub-optimal solution to Problem (30)

1. Choose $\eta_{\text{acc}} > 0$, $I_{\text{max}} > 0$, and $\{\mathbf{u}_k, \mathbf{w}_k, \mathbf{w}_{k,m}\}$
2. $i = 0$ and $f^{(0)} = f(\{\text{SINR}_k\})$
3. **repeat**
4. $i = i + 1$
5. Update $\{\mathbf{u}_k\}$ by solving (40)
6. Update $\{\mathbf{w}_k\}$ as in (44)
7. Update $\{\mathbf{w}_{k,m}\}$ as explained in Sec. IV-C
8. $f^{(i)} = f(\{\text{SINR}_k\})$
9. **until** $f^{(i)} - f^{(i-1)} < \eta_{\text{acc}} f^{(i)}$ or $i = I_{\text{max}}$

Notice that the objective function in (32) is non-concave in the optimization variables, while the constraint C3 is non-convex.

To proceed, Problem (32) is first recast as

$$\begin{aligned} & \max_{\{\mathbf{u}_k, x_k\}} f(\mathbf{x}) \\ & \text{s.t. C1, C2, C3} \end{aligned} \quad (33)$$

$$\text{C5: } \frac{\mathbf{u}_k^H \Psi_{k,1} \mathbf{u}_k}{\mathbf{u}_k^H \Psi_{k,2} \mathbf{u}_k + \sigma_{z,k}^2 \|\mathbf{w}_k\|^2} \geq x_k, \quad \forall k$$

where x_1, \dots, x_K are non-negative auxiliary variables and $\mathbf{x} = (x_1 \cdots x_K)^T$. Next, a convex restriction of C3 and C5 is derived. Let $\{\tilde{\mathbf{u}}_k, \tilde{x}_k\}$ be the optimized variables at the previous iteration of Algorithm 1. Then, upon defining

$$\begin{aligned} \Upsilon_{k,m} &= \frac{|\beta_{k,m,0}|^2}{\sigma_{z,k,m}^2 \|\mathbf{w}_{k,m}\|^2} \\ & \times \mathbf{G}_{k,m}(\bar{\phi}_{m,0}, \phi_{m,0}) \mathbf{w}_{k,m} \mathbf{w}_{k,m}^H \mathbf{G}_{k,m}^H(\bar{\phi}_{m,0}, \phi_{m,0}) \\ & + \sum_{q=1}^{Q_m} \frac{\sigma_{\beta,k,m,q}^2}{\sigma_{z,k,m}^2 \|\mathbf{w}_{k,m}\|^2} \\ & \times \mathbf{G}_{k,m}(\bar{\phi}_{m,q}, \phi_{m,q}) \mathbf{w}_{k,m} \mathbf{w}_{k,m}^H \mathbf{G}_{k,m}^H(\bar{\phi}_{m,q}, \phi_{m,q}) \end{aligned} \quad (34)$$

we have [61]

$$\begin{aligned} \text{SNR}_{k,m} &\geq \tilde{\mathbf{u}}_k^H \Upsilon_{k,m} \tilde{\mathbf{u}}_k + 2\Re\{\tilde{\mathbf{u}}_k^H \Upsilon_{k,m} (\mathbf{u}_k - \tilde{\mathbf{u}}_k)\} \\ &= 2\Re\{\tilde{\mathbf{u}}_k^H \Upsilon_{k,m} \mathbf{u}_k\} - \tilde{\mathbf{u}}_k^H \Upsilon_{k,m} \tilde{\mathbf{u}}_k \end{aligned} \quad (35)$$

where the inequality follows from the fact that $\text{SNR}_{k,m} = \mathbf{u}_k^H \Upsilon_{k,m} \mathbf{u}_k$ is a convex function of \mathbf{u}_k . At this point, we replace C3 with the following tighter constraint

$$\text{C3R: } 2\Re\{\tilde{\mathbf{u}}_k^H \Upsilon_{k,m} \mathbf{u}_k\} - \tilde{\mathbf{u}}_k^H \Upsilon_{k,m} \tilde{\mathbf{u}}_k \geq \rho_{k,m}, \quad \forall m, k. \quad (36)$$

As to C5, first notice that it is active only when $x_k > 0$, and, in this case, it can be rewritten as

$$g_k(\mathbf{u}_k, x_k) \geq \mathbf{u}_k^H \Psi_{k,2} \mathbf{u}_k + \sigma_{z,k}^2 \|\mathbf{w}_k\|^2 \quad (37)$$

where $g_k(\mathbf{u}_k, x_k) = \frac{1}{x_k} \mathbf{u}_k^H \Psi_{k,1} \mathbf{u}_k$. We now have the following result, whose proof is provided in Appendix B.

Proposition 3. Let $\Psi \in \mathbb{C}^{N \times N}$, with $\Psi \succeq 0$, and $g(\mathbf{u}, x) = \frac{1}{x} \mathbf{u}^H \Psi \mathbf{u}$; then, $g: \mathbb{C}^N \times (0, \infty) \rightarrow \mathbb{R}$ is convex.

Then, exploiting the convexity of g_k , we have

$$\begin{aligned} g_k(\mathbf{u}_k, x_k) &\geq g_k(\tilde{\mathbf{u}}_k, \tilde{x}_k) + \Re\left\{\left(\frac{\partial g_k(\tilde{\mathbf{u}}_k, \tilde{x}_k)}{\partial \mathbf{u}_k}\right)^H \right. \\ & \quad \left. \times (\mathbf{u}_k - \tilde{\mathbf{u}}_k) + \frac{\partial g_k(\tilde{\mathbf{u}}_k, \tilde{x}_k)}{\partial x_k} (x_k - \tilde{x}_k)\right\} \\ &= \frac{2}{\tilde{x}_k} \Re\{\tilde{\mathbf{u}}_k^H \Psi_{k,1} \mathbf{u}_k\} - \frac{x_k}{\tilde{x}_k^2} \tilde{\mathbf{u}}_k^H \Psi_{k,1} \tilde{\mathbf{u}}_k \end{aligned} \quad (38)$$

if $\tilde{x}_k > 0$, where the partial derivatives of g_k are available from (58a). Therefore, from (37) and (38), we can replace C5 with the following tighter constraint

$$\text{C5R: } \begin{cases} \frac{2}{\tilde{x}_k} \Re\{\tilde{\mathbf{u}}_k^H \Psi_{k,1} \mathbf{u}_k\} - \frac{x_k}{\tilde{x}_k^2} \tilde{\mathbf{u}}_k^H \Psi_{k,1} \tilde{\mathbf{u}}_k \\ \geq \mathbf{u}_k^H \Psi_{k,2} \mathbf{u}_k + \sigma_{z,k}^2 \|\mathbf{w}_k\|^2, & \forall k: \tilde{x}_k > 0 \\ x_k = 0, & \forall k: \tilde{x}_k = 0. \end{cases} \quad (39)$$

We now propose to solve the following restricted problem

$$\max_{\{\mathbf{u}_k, x_k\}} f(\mathbf{x}), \quad \text{s.t. C1, C2, C3R, C5R.} \quad (40)$$

If f is concave, then (40) is a convex problem and can be solved by using standard optimization techniques [61]; in this case, a solution to (40) is a feasible point for (32); also, after updating $\{\mathbf{u}_k, x_k\}$ as in (40), the value of the objective function in (32) is not decreased.

If f is not concave but it can be minorized at any point by a concave function, we can sub-optimally solve Problem (40) via a minorization-maximization algorithm [58]. Specifically, starting from $\mathbf{x}^{(0)} = (\tilde{x}_1, \dots, \tilde{x}_K)^T$, a sequence of feasible points is generated by the following induction: given $\mathbf{x}^{(i-1)}$, choose $\mathbf{x}^{(i)}$ as the solution to the following convex problem

$$\max_{\{\mathbf{u}_k, x_k\}} \zeta(\mathbf{x}|\mathbf{x}^{(i-1)}), \quad \text{s.t. C1, C2, C3R, C5R.} \quad (41)$$

The solution to (41) is a feasible point for (32); also, after updating $\{\mathbf{u}_k, x_k\}$ as in (41), we have

$$f(\mathbf{x}^{(i)}) \geq \zeta(\mathbf{x}^{(i)}|\mathbf{x}^{(i-1)}) \geq \zeta(\mathbf{x}^{(i-1)}|\mathbf{x}^{(i-1)}) = f(\mathbf{x}^{(i-1)}) \quad (42)$$

whereby $\{f(\mathbf{x}^{(i)})\}_{i \in \mathbb{N}}$ is a non decreasing sequence. Since solving (40) is part of an alternating-maximization algorithm, it is not necessary to iterate the maximization of $g(\mathbf{x}|\mathbf{x}^{(i-1)})$ in (41) until convergence and we can just proceed to update the other block variables $\{\mathbf{u}_k\}$ and $\{\mathbf{w}_{k,m}\}$ after only one or few steps of inner minorization-maximization. The assumption that $f(\cdot)$ be (locally) minorized by a concave function is quite mild in practice, and, indeed, Sec. III-A lists several meaningful merit functions possessing such property. Clearly, a possible difficulty may come from finding the appropriate surrogate function that minorizes the desired objective function. Indeed, a good surrogate function should try to closely follow the shape of the objective function so as to yield a faster convergence rate in the minorization-maximization algorithm; on the other hand, it should be also possess a simple structure to reduce the computational cost per iteration.

B. Update of the Radar Receive Filters

The filter \mathbf{w}_k only comes into play in the objective function. Since f is increasing, the optimal \mathbf{w}_k must maximize SINR_k . This problem is separable for each user and subcarrier and admits a closed form solution. Indeed, we have

$$\begin{aligned} \text{SINR}_k &= \frac{\sigma_{\eta,k}^2 \mathbf{w}_k^H \mathbf{G}_k(\psi_k) \mathbf{u}_k \mathbf{u}_k^H \mathbf{G}_k(\psi_k) \mathbf{w}_k}{\mathbf{w}_k^H \Phi_k(\mathbf{u}_k) \mathbf{w}_k} \\ &\leq \sigma_{\eta,k}^2 \mathbf{u}_k^H \mathbf{G}_k^H(\psi_k) \Phi_k^{-1}(\mathbf{u}_k) \mathbf{G}_k(\psi_k) \mathbf{u}_k \end{aligned} \quad (43)$$

where $\Phi_k(\mathbf{u}_k) = \sum_{j=1}^J \sigma_{\alpha,k,j}^2 \mathbf{G}_k(\theta_j) \mathbf{u}_k \mathbf{u}_k^H \mathbf{G}_k(\theta_j) + \sigma_{z,k}^2 \mathbf{I}_{N_r}$, and the upper bound is achieved (up to an irrelevant scaling factor) when [62]

$$\mathbf{w}_k = \Phi_k^{-1}(\mathbf{u}_k) \mathbf{G}_k(\psi_k) \mathbf{u}_k. \quad (44)$$

C. Update of the User Receive Filters

Let $\Pi_{k,m}^d$ be equal to the projector onto the orthogonal complement of the subspace spanned by the vectors $\{\mathbf{g}_{k,m}(\bar{\phi}_{m,q})\}_{q=1}^{Q_m}$, if $Q_m > 0$, and to \mathbf{I}_{N_m} otherwise; also, let $\Pi_{k,m}^i$ be equal to the projector onto the orthogonal complement of the subspace spanned by $\mathbf{g}_{k,m}(\bar{\phi}_{m,0})$, if $|\beta_{k,m,0}| > 0$, and to \mathbf{I}_{N_m} otherwise; finally, let

$$\begin{aligned} \Xi_{k,m} &= \frac{|\beta_{k,m,0}|^2}{\sigma_{z,k,m}^2} \mathbf{G}_{k,m}(\bar{\phi}_{m,0}, \phi_{m,0}) \mathbf{u}_k \mathbf{u}_k^H \mathbf{G}_{k,m}^H(\bar{\phi}_{m,0}, \phi_{m,0}) \\ &+ \sum_{q=1}^{Q_m} \frac{\sigma_{\beta,k,m,q}^2}{\sigma_{z,k,m}^2} \mathbf{G}_{k,m}(\bar{\phi}_{m,q}, \phi_{m,q}) \mathbf{u}_k \mathbf{u}_k^H \mathbf{G}_{k,m}^H(\bar{\phi}_{m,q}, \phi_{m,q}). \end{aligned} \quad (45)$$

Then, we have the following result, whose proof is reported in Appendix C.

Proposition 4. *If Problem (30) is feasible, then the optimal $\mathbf{w}_{k,m}$ is proportional to the eigenvector corresponding to the largest eigenvalue of $\Xi_{k,m}^d = (\mathbf{I}_T \otimes \Pi_{k,m}^d) \Xi_{k,m} (\mathbf{I}_T \otimes \Pi_{k,m}^d)$, if $\kappa_{k,m} = \infty$, and of $\Xi_{k,m}^i = (\mathbf{I}_T \otimes \Pi_{k,m}^i) \Xi_{k,m} (\mathbf{I}_T \otimes \Pi_{k,m}^i)$, if $\kappa_{k,m} = 0$, for $m = 1, \dots, M$ and $k = 1, \dots, K$.*

According to Proposition 4, we compute here two candidate solutions for $\mathbf{w}_{k,m}$; one solution is proportional to the eigenvector corresponding to the maximum eigenvalue of $\Xi_{k,m}^d$ (so that $\kappa_{k,m} = \infty$), while the other to the eigenvector corresponding to the maximum eigenvalue of $\Xi_{k,m}^i$ (so that $\kappa_{k,m} = 0$). When both solutions are feasible, the one providing the lower error probability is selected; otherwise, we simply keep the one which is feasible.

Notice in passing that, by leveraging Proposition 4, we can also obtain the following side result on the feasibility of C3, whose proof is reported in Appendix D.

Proposition 5. *A necessary condition for the feasibility of C3 in Problem (30) is $\|\mathbf{U}_k^H \mathbf{s}_k^*(\phi_{m,0})\| \neq 0$, if $\kappa_{k,m} = \infty$, and $\max_{q \in \{1, \dots, Q_m\}} \|\mathbf{U}_k^H \mathbf{s}_k^*(\phi_{m,q})\| > 0$, if $\kappa_{k,m} = 0$, for*

$m = 1, \dots, M$ and $k = 1, \dots, K$. If $\text{Rank}\{\mathbf{U}_k\} = N_t$, a sufficient condition for the feasibility of C3 in Problem (30) is

$$\lambda_{\min}(\mathbf{U}_k \mathbf{U}_k^H) \geq \begin{cases} \frac{\rho_{k,m}^d \sigma_{z,k,m}^2 / N_t}{|\beta_{k,m,0}|^2 \mathbf{g}^H(\bar{\phi}_{m,0}) \Pi_{k,m}^d \mathbf{g}_{k,m}(\bar{\phi}_{m,0})}, & \text{if } \kappa_{k,m} = \infty \\ \frac{\rho_{k,m}^i \sigma_{z,k,m}^2 / N_t}{\max_q |\beta_{k,m,q}|^2 \mathbf{g}^H(\bar{\phi}_{m,q}) \Pi_{k,m}^i \mathbf{g}_{k,m}(\bar{\phi}_{m,q})}, & \text{if } \kappa_{k,m} = 0 \end{cases} \quad (46)$$

for $m = 1, \dots, M$ and $k = 1, \dots, K$.

D. Selection of the Starting Point

Next we outline a possible method to obtain a starting point for Algorithm 1. To this end, consider the following problem

$$\begin{aligned} &\max_{t, \{\mathbf{u}_k\}, \{\mathbf{w}_{k,m}\}} t \\ &\text{s.t. C1, C2, C4} \\ &\quad \overline{\text{C3}}: \text{SNR}_{k,m}(\mathbf{u}_k, \mathbf{w}_{k,m}) / \rho_{k,m} \geq t. \end{aligned} \quad (47)$$

If the optimal t is not lower than 1, then the corresponding variables $\{\mathbf{u}_k\}$ and $\{\mathbf{w}_{k,m}\}$ together with the radar receive filters $\{\mathbf{w}_k\}$ obtained as by-product from (44) are a feasible point for Algorithm 1. Since (47) is an NP-hard program [63], we resort here to an alternating maximization of the block variables $\{t, \mathbf{u}_k\}$ and $\{\mathbf{w}_{k,m}\}$. Given $\{\mathbf{w}_{k,m}\}$, we can update $\{t, \mathbf{u}_k\}$ by solving the following problem

$$\max_{t, \{\mathbf{u}_k\}} t, \quad \text{s.t. C1, C2, } \overline{\text{C3}}, \quad (48)$$

which can be tackled, similarly to what was done for Problem (33), by introducing a convex restriction of $\overline{\text{C3}}$. Also, given $\{t, \mathbf{u}_k\}$, we can update $\{\mathbf{w}_{k,m}\}$ as described in Sec. IV-C. At the beginning, $\{\mathbf{u}_k\}$ can be randomly selected and normalized to meet C1. Also, $\{\mathbf{w}_{k,m}\}$ can be initialized as follows. First we randomly decide whether user k will utilize the direct path or the indirect paths (if both present) on the k -th subcarrier; if the direct path is used, then $\mathbf{w}_{k,m} = (\mathbf{I}_T \otimes \Pi_{k,m}^d)(\mathbf{I}_T \otimes \mathbf{g}_{k,m}(\bar{\phi}_{m,0}))$, otherwise, $\mathbf{w}_{k,m} = (\mathbf{I}_T \otimes \Pi_{k,m}^i)(\mathbf{I}_T \otimes \mathbf{g}_{k,m}(\bar{\phi}_{m,q}))$, where $\hat{q} = \max_{q \in \{1, \dots, Q_m\}} \sigma_{\beta,k,m,q}^2$.

V. NUMERICAL ANALYSIS

We consider an OFDM system using a power $\mathcal{P} = 20$ dBW on the shared subcarriers. The center frequency of the k -th subcarriers is $f_k = f_0 + (k-1)\Delta f$, where $f_0 = 2$ GHz and $\Delta f = 100$ KHz, while each array has a uniform element spacing of $c/(2 \max_k f_k)$. At the communication side, we set $\sigma_{z,k,m}^2 = -150$ dBW and $\epsilon_{k,m} = \epsilon$. The users have either one direct path or two indirect paths (they will be referred to as the direct and indirect users, respectively) with the corresponding angles of arrival/departure sampled from the uniform distribution on $[-\pi/3, \pi/3]$. The response of the direct path is set to have $|\beta_{k,m,0}|^2 = -130$ dB, while that of the indirect paths is chosen to have $\sum_{q=1}^{Q_m} \sigma_{\beta,k,m,q}^2 = -130$ dBW. Unless otherwise stated, we consider two direct and two indirect users. At the radar side, a different direction randomly chosen in

Table I

Parameter	Value	Description
N_t	11	number of transmit antennas
N_r	4	number of radar receive antennas
N_c	4	number of user receive antennas
K	4	number of subcarriers
T	2	number of time slots
D	2	constellation size

$[-\pi/3, \pi/3]$ is inspected on each subcarrier. Also, we set $\sigma_{z,k}^2 = -150$ dBW, $\sigma_{\eta,k}^2 = -160$ dB, and $J = 4$, while the strength of each clutter element is assumed to be equal and adjusted according to a given signal-to-clutter ratio (SCR), defined as⁸ $\text{SCR} = \sigma_{\eta,k}^2 / \sum_{j=1}^J \sigma_{\alpha,k,j}^2$. As to the transmit beampattern, we set $\delta_{k,\ell} = \delta$ and $L_k = L$, while the protected directions are randomly chosen $[-\pi/3, \pi/3]$. Unless otherwise stated, we consider $L = 6$. The other parameters are given in Table I. Algorithm 1 is implemented with $\eta_{\text{acc}} = 10^{-4}$ and $I_{\text{max}} = 2000$, while the block variables $\{\mathbf{u}_k\}$, $\{\mathbf{w}_k\}$, and $\{\mathbf{w}_{k,m}\}$ are initialized as in Sec. IV-D; finally, the auxiliary variable \tilde{x}_k in Problem (40) is initialize to SINR_k .

A. Examples

First we examine the interplay between the radar and communication operations, which compete here for the same physical resources. We consider three radar merit functions: the arithmetic mean, i.e., the merit function in (12) with $p = 1$; the detection probability in (17) with $P_{\text{fa},k} = 10^{-4}$; and the relative entropy in (20) with $\omega_k = 0$. In all cases, we set $\mu_k = 1/K$. Fig. 1 reports these radar merit functions versus the constraint ϵ on the user error rate for $\delta = 10^{-6}, 10^{-3}, 1$; two SCRs are considered, namely, -20 dB and 20 dB. The curves are obtained by averaging over 10 problem instances. A lower objective is attained when δ and/or SCR decrease, since the system consumes more degrees of freedom to reduce the power leakage towards the clutter and the protected directions; notice here that $\delta = 1$ is tantamount to removing C2. There is an evident trade-off between the radar and communication performance; in particular, the radar performance sharply drops when ϵ gets lower than 10^{-5} , as most of the system resources are employed for data transmission; instead, the communication function only marginally restrains the radar performance if ϵ is larger than $10^{-3.5}$.

For one problem instance included in the top-left plot of Fig. 1, we now visualize the optimized transmit and receive beampatterns in one subcarrier when $\epsilon = 10^{-5}$ and $\delta = 10^{-6}$. The transmit beampattern is defined as in (10), while the radar and user receive beampatterns are $\|\mathbf{W}_k^H \mathbf{g}_k(\xi)\|^2/T$ and $\|\mathbf{W}_{k,m}^H \mathbf{g}_{k,m}(\xi)\|^2/T$, respectively. Fig. 2 depicts the transmit beampattern (black, solid); the vertical lines indicate the locations of the clutter (orange, dashed) and protected directions (red, dash dot), in the top plot, and the locations of the radar target (green, solid) and of the direct (blue, dotted) and indirect

⁸The parameter SCR is the ratio between the power of the target response and the sum-power of the response of each clutter element; accordingly, it does not account for the combined effects of the transmit and receive filters.

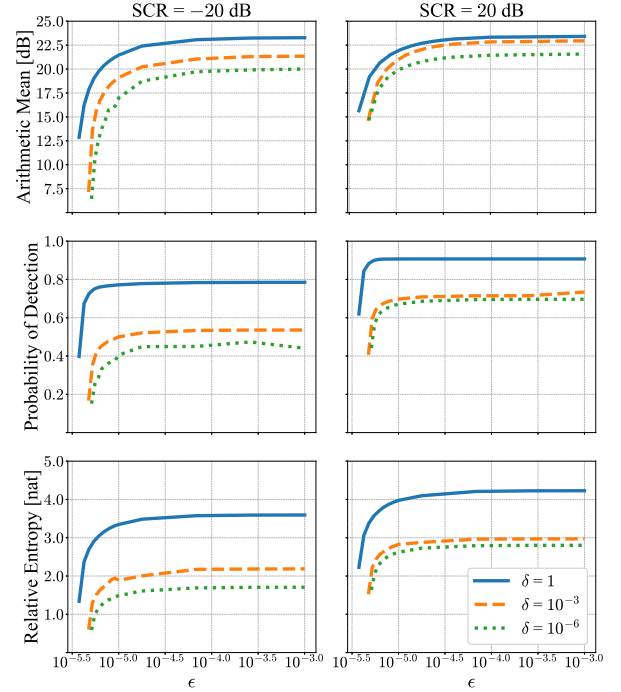


Figure 1. Arithmetic mean of the radar SINRs (top), probability of detection with $P_{\text{fa},k} = 10^{-4}$ (middle), and the relative entropy with $\omega_k = 0$ (bottom) vs. the constraint ϵ on the user error rate for $\delta = 10^{-6}, 10^{-3}, 1$ when SCR of -20 dB (left) and 20 dB (right).

(blue, solid) users, in the bottom plot. It is verified by inspection that the transmit beampattern peaks at the target location and has nulls at the protected directions. The indirect users are allocated significant power since they require a large SNR to achieve the specified error rate, while it suffices to serve the direct users by sidelobes—the required $\epsilon = 10^{-5}$ corresponds to $\text{SNR} \approx 10$ dB for direct users and $\text{SNR} \approx 40$ dB for indirect users. For the same scenario considered in Fig. 2, Fig. 3 shows (top) the radar receive beampattern with clutter (orange, dashed) and target (green, solid) directions superimposed and (bottom) the receive beampattern of one indirect user with the direction of the received paths superimposed. The radar receive beampattern peaks at the target location and, together with the transmit beampattern, concurs to mitigate the clutter: indeed, for each clutter direction, we may have a null in the transmit beampattern, a null in the receive beampattern, or sufficiently low values in both beampatterns. The user's receive beampattern instead only emphasizes the two indirect paths.

For another problem instance included in the top-left plot of Fig. 1, Fig. 4 shows the effect of decreasing ϵ (the constraint on user error rate) on the transmit beampattern obtained in the first subcarrier. Here the line styles match those of Fig. 2 and $\delta = 10^{-6}$. When $\epsilon = 10^{-2}$, the mainlobe is centered on the target. Instead, when $\epsilon = 10^{-5}$, there are three lobes of similar height directed toward the target and indirect users. Some of the power that was directed toward the radar in the former case has been reallocated to the indirect users in the latter.

We now study the mismatch loss when the true SCR is different from the one employed for design. Fig. 5 reports the arithmetic mean of the radar SINRs versus the true SCR,

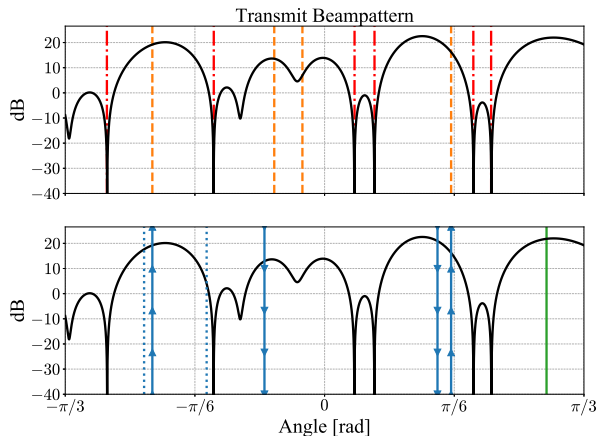


Figure 2. Transmit beampattern (black, solid) on one subcarrier for one problem instance included in the top-left plot of Fig. 1, when $\epsilon = 10^{-5}$, $\delta = 10^{-6}$, and $\text{SCR} = -20$ dB. Here, the top plot shows the transmit beampattern along with the clutter (orange, dashed) and protected (red, dash dot) directions, while the bottom plot shows the transmit beampattern along with the target (green, solid) and user (blue) directions. There are two direct (blue, dotted) and two indirect (blue, solid) users with two indirect paths each; the indirect users are distinguished by the markers.

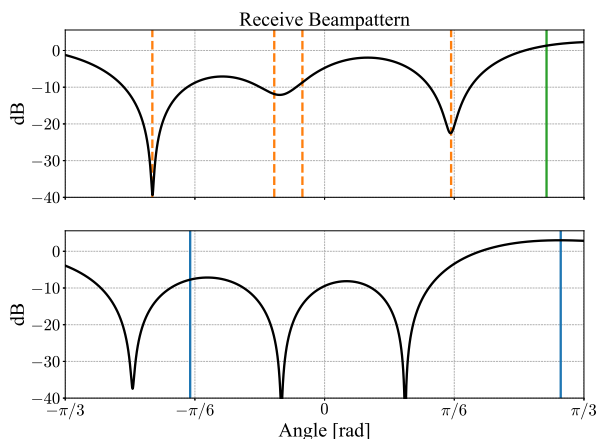


Figure 3. Receive beampatterns (black, solid) on one subcarrier for one problem instance included in the top-left plot of Fig. 1, when $\epsilon = 10^{-5}$, $\delta = 10^{-6}$, and $\text{SCR} = -20$ dB. The top plot shows the radar receive beampattern along with the target (green, solid) and clutter (orange, dashed) directions; the bottom plot shows to the receive beampattern of one indirect user along with its receive directions (blue, solid).

when $\epsilon = 10^{-5}$, $\delta = 10^{-6}$, and the system is optimized for a nominal SCR of $-20, -10, 0, 10, 20$ dB. Using a nominal SCR of -20 dB yields a quite robust design; indeed, the optimization prioritizes nulling the clutter directions, thus making the true strength of the clutter less consequential. When instead the design SCR is 20 dB, the objective function decays rapidly as the true SCR decreases, while becoming only slightly favored when the true SCR is 20 dB or greater.

Next, we vary the number of connected users when $\epsilon = 10^{-5}$, $\delta = 10^{-4}$, $\text{SCR} = -20$ dB, and $L \in \{0, 2, 4\}$. Fig. 6 reports the arithmetic mean of the radar SINRs when there are 4 direct users and M is increased up to 8 by adding either indirect users (dashed) or direct users (solid). Adding indirect users causes a severe performance loss; indeed, for the same

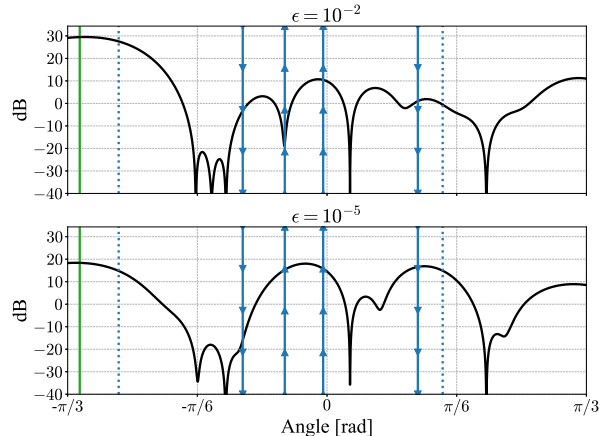


Figure 4. Transmit beampattern (black, solid) on one subcarrier for one problem instance in the top-left plot of Fig. 1, when $\epsilon = 10^{-2}, 10^{-5}, \delta = 10^{-6}$ and $\text{SCR} = -20$ dB. The target (green, solid) and user (blue) directions are superimposed, including two direct (blue, dotted) and two indirect (blue, solid) users with two indirect paths each. The indirect users are distinguished by the markers.

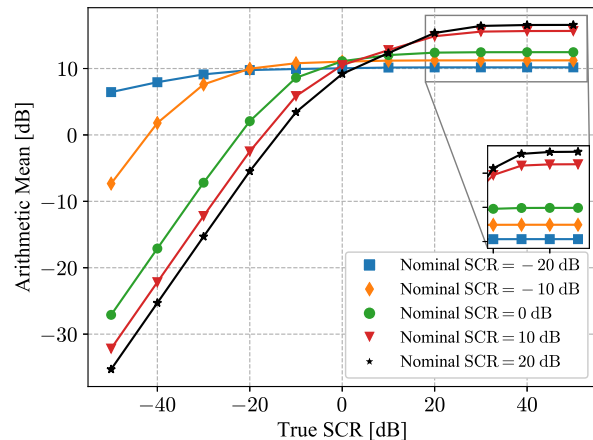


Figure 5. Arithmetic mean of the radar SINRs versus the true SCR, when $\epsilon = 5 \times 10^{-6}$, $\delta = 10^{-3}$, and the system is optimized for an SCR of $-20, -10, 0, 10, 20$ dB.

error rate, the indirect users requires more physical resources than the direct ones to counteract the channel fading.

Finally, we consider the merit function in (12), and we assess the effect of changing p on the individual radar SINRs on each subcarrier. For $p \in \{-20, -10, -5, -1, 1\}$, we run the Algorithm 1 for 10 instances when $\epsilon = 4.75 \times 10^{-5}$, $\delta = 10^{-3}$, and $\text{SCR} = -20$ dB; then we compute the average highest SINR obtained by a subcarrier in each instance, the second-highest SINR, and so on. Fig. 7 reports these averages for each p . It is seen a smaller p better safeguards the radar operation in the less favorable subcarrier at the price of some performance loss in the most favorable one.

VI. CONCLUSIONS

In this manuscript, we have considered an OFDM-DFRC system employing a DPSK modulation. We have selected the transmit waveforms and the receive filters to maximize the radar performance under constraints on the average radiated

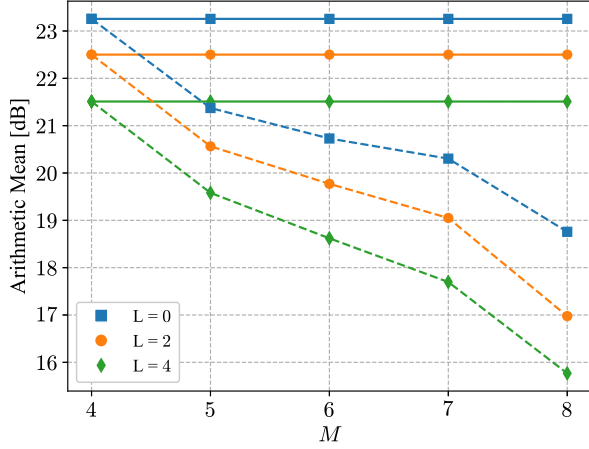


Figure 6. Arithmetic mean of the radar SINRs vs number of users M for $L = 0, 2, 4$ when $\epsilon = 10^{-5}$, $\delta = 10^{-4}$, and $\text{SCR} = -20$ dB. The solid and dashed lines are generated by adding direct and indirect users, respectively.

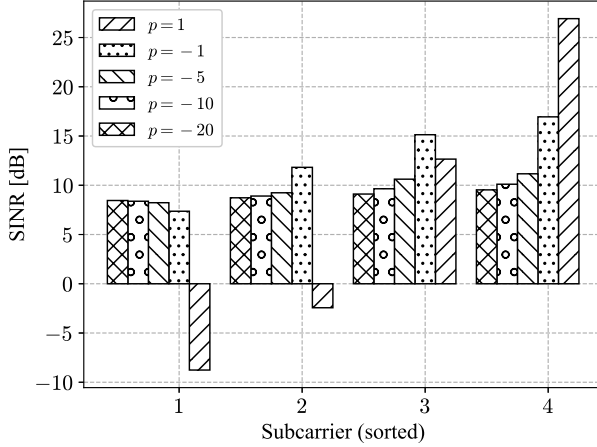


Figure 7. p -power mean of the radar SINRs versus (sorted) subcarrier for $p = -20, -10, -5, -1, 1$, when $\epsilon = 4.75 \times 10^{-5}$, $\delta = 10^{-3}$, and $\text{SCR} = -20$ dB. Here, subcarrier 1 corresponds to the subcarrier with minimum SINR, and 4 corresponds to that with maximum SINR.

power, the error rate of each user, and the beam pattern level towards specific directions. The system design results in a non-convex problem, which has been suboptimally solved via an iterative procedure based upon an alternating maximization of the involved variables, a convex restriction of the feasible search set, and the minorization-maximization algorithm. Remarkably, the proposed procedure can be used for a broad family of radar merit functions. The numerical analysis has illustrated the achievable system tradeoffs and the effect of the prior uncertainty on the target strength.

Future developments may consider the use of reconfigurable intelligent surfaces to reach blind spots or create additional indirect paths, and the use of a differential space-time-frequency code to exploit frequency diversity. Also, the system design when the users simultaneously exploit both direct and indirect signals is an open problem that requires further investigation.

APPENDIX

Here we provide the proofs of Propositions 1, 3, 4, and 5.

A. Proof of Proposition 1

Let $y = \sum_{i=1}^K \mu_i \gamma(x_i)$, so that $f(\mathbf{x}) = \gamma^{-1}(y)$. Exploiting the formula for the derivative of the inverse function, we have

$$\frac{\partial f(\mathbf{x})}{\partial x_i} = \frac{\mu_i \gamma'(x_i)}{\gamma'(\gamma^{-1}(y))} \quad (49a)$$

$$\frac{\partial^2 f(\mathbf{x})}{\partial x_i^2} = \frac{\mu_i \gamma''(x_i)}{\gamma'(\gamma^{-1}(y))} - \frac{\mu_i^2 [\gamma'(x_i)]^2 \gamma''(\gamma^{-1}(y))}{[\gamma'(\gamma^{-1}(y))]^3} \quad (49b)$$

$$\frac{\partial^2 f(\mathbf{x})}{\partial x_i \partial x_j} = -\frac{\mu_i \mu_j \gamma'(x_i) \gamma'(x_j) \gamma''(\gamma^{-1}(y))}{[\gamma'(\gamma^{-1}(y))]^3} \quad (49c)$$

so that the Hessian matrix is

$$\begin{aligned} \nabla_f^2(\mathbf{x}) &= \frac{1}{\gamma'(\gamma^{-1}(y))} \text{diag}(\{\mu_i \gamma''(x_i)\}) - \frac{\gamma''(\gamma^{-1}(y))}{[\gamma'(\gamma^{-1}(y))]^3} \\ &\quad \times \begin{pmatrix} \mu_1 \gamma'(x_1) \\ \vdots \\ \mu_K \gamma'(x_K) \end{pmatrix} (\mu_1 \gamma'(x_1) \cdots \mu_K \gamma'(x_K)) \end{aligned} \quad (50)$$

that is negative semidefinite for any $\mathbf{x} \in \bar{\mathbb{R}}^K$ if and only if

$$\begin{aligned} \mathbf{z}^T \nabla_f^2(\mathbf{x}) \mathbf{z} &= \frac{1}{[\gamma'(\gamma^{-1}(y))]^3} \left([\gamma'(\gamma^{-1}(y))]^2 \right. \\ &\quad \left. \times \sum_{i=1}^K \mu_i \gamma''(x_i) z_i^2 - \gamma''(\gamma^{-1}(y)) \left(\sum_{i=1}^K \mu_i \gamma'(x_i) z_i \right)^2 \right) \leq 0 \end{aligned} \quad (51)$$

for all $\mathbf{z} \in \mathbb{R}^K$ and any $\mathbf{x} \in \bar{\mathbb{R}}^K$.

In order to prove (51), we follow and generalize the approach in [45, Ch. III, Sec. 16], where the convexity of f (instead of the concavity) is proven under the condition that $\gamma \in C^4$ is strictly positive, strictly increasing, and strictly convex. In particular, since either $\gamma'(x) > 0$ and $\gamma''(x) < 0$ for all $x \in \bar{\mathbb{R}}$, or $\gamma'(x) < 0$ and $\gamma''(x) > 0$ for all $x \in \bar{\mathbb{R}}$, inequality (51) holds if and only if, for any $\mathbf{x} \in \bar{\mathbb{R}}^K$,

$$\frac{[\gamma'(\gamma^{-1}(y))]^2}{|\gamma''(\gamma^{-1}(y))|} \geq \frac{\left(\sum_{i=1}^K \mu_i \gamma'(x_i) z_i \right)^2}{\sum_{i=1}^K \mu_i |\gamma''(x_i)| z_i^2}, \quad \forall \mathbf{z} \in \mathbb{R}^K. \quad (52)$$

Now, by the Cauchy-Schwarz inequality, we have that

$$\begin{aligned} \left(\sum_{i=1}^K \mu_i \gamma'(x_i) z_i \right)^2 &= \left(\sum_{i=1}^K z_i \sqrt{\mu_i |\gamma''(x_i)|} \sqrt{\frac{\mu_i [\gamma'(x_i)]^2}{|\gamma''(x_i)|}} \right)^2 \\ &\leq \sum_{i=1}^K \mu_i |\gamma''(x_i)| z_i^2 \sum_{i=1}^K \mu_i \frac{[\gamma'(x_i)]^2}{|\gamma''(x_i)|} \end{aligned} \quad (53)$$

with equality if and only if z_i is proportional to $\frac{\gamma'(x_i)}{|\gamma''(x_i)|}$. Therefore, condition (52) holds if and only if

$$\frac{[\gamma'(\gamma^{-1}(y))]^2}{|\gamma''(\gamma^{-1}(y))|} \geq \sum_{i=1}^K \mu_i \frac{[\gamma'(x_i)]^2}{|\gamma''(x_i)|}, \quad \forall \mathbf{x} \quad (54)$$

which, upon defining $g(y) = [\gamma'(\gamma^{-1}(y))]^2 / [|\gamma''(\gamma^{-1}(y))|]$ and recalling that $y = \sum_{i=1}^K \mu_i \gamma(x_i)$, becomes

$$g\left(\sum_{i=1}^K \mu_i \gamma(x_i)\right) \geq \sum_{i=1}^K \mu_i g(x_i), \quad \forall \mathbf{x} \in \bar{\mathbb{R}}^K. \quad (55)$$

This is a concavity condition on g that, since $\gamma \in C^4$, is satisfied if and only if $g''(y) \leq 0$, for all y . Finally, since

$$g'(y) = -\frac{d}{dx} \frac{\gamma'(x)}{\gamma''(x)} \Big|_{x=\gamma^{-1}(y)} - 1 \quad (56a)$$

$$g''(y) = -\frac{1}{\gamma'(x)} \frac{d^2}{dx^2} \frac{\gamma'(x)}{\gamma''(x)} \Big|_{x=\gamma^{-1}(y)} \quad (56b)$$

if $\gamma'(x) > 0$ and $\gamma''(x) < 0$ for all $x \in \bar{\mathbb{R}}$, and

$$g'(y) = \frac{d}{dx} \frac{\gamma'(x)}{\gamma''(x)} \Big|_{x=\gamma^{-1}(y)} + 1 \quad (57a)$$

$$g''(y) = \frac{1}{\gamma'(x)} \frac{d^2}{dx^2} \frac{\gamma'(x)}{\gamma''(x)} \Big|_{x=\gamma^{-1}(y)} \quad (57b)$$

if $\gamma'(x) < 0$ and $\gamma''(x) > 0$ for all $x \in \bar{\mathbb{R}}$, we have that g is concave if and only if γ'/γ'' is convex.

B. Proof of Proposition 3

The function g is twice-differentiable with

$$\nabla_g(\mathbf{u}, x) = \left(-\frac{2}{x} \Psi \mathbf{u}, -\frac{1}{x^2} \mathbf{u}^H \Psi \mathbf{u} \right) \quad (58a)$$

$$\nabla_g^2(\mathbf{u}, x) = \frac{2}{x} \begin{pmatrix} \Psi & -\frac{1}{x} \Psi \mathbf{u} \\ -\frac{1}{x} \mathbf{u}^H \Psi & \frac{1}{x^2} \mathbf{u}^H \Psi \mathbf{u} \end{pmatrix}. \quad (58b)$$

Since $\Psi \succeq 0$ and

$$(\mathbf{I}_N - \Psi \Psi^\dagger) \left(-\frac{1}{x} \Psi \mathbf{u} \right) = \mathbf{0}_N \quad (59a)$$

$$\frac{1}{x^2} \mathbf{u}^H \Psi \mathbf{u} - \left(\frac{1}{x} \mathbf{u}^H \Psi \right) \Psi^\dagger \left(\frac{1}{x} \Psi \mathbf{u} \right) = 0 \quad (59b)$$

we conclude that $\nabla_g^2(\mathbf{u}, x) \succeq 0$ for any $\mathbf{u} \in \mathbb{C}^N$ and $x > 0$ [61, Sec. A.5.5], so that g is convex.

C. Proof of Proposition 4

The filter $\mathbf{w}_{k,m}$ only comes into play in C3 and C4. Assume first that $\kappa_{k,m} = \infty$. For any feasible \mathbf{u}_k , the optimal $\mathbf{w}_{k,m}$ must maximize $\text{SNR}_{k,m}$ under the constraint set $\mathcal{W}_{k,m}^d = \{\mathbf{w}_{k,m} \in \mathbb{C}^{TN_m} : \kappa_{k,m} = \infty\}$. Notice now that

$$\begin{aligned} \max_{\mathbf{w}_{k,m} \in \mathcal{W}_{k,m}^d} \text{SNR}_{k,m} &= \max_{\mathbf{w}_{k,m} \in \mathcal{W}_{k,m}^d} \frac{\mathbf{w}_{k,m}^H \Xi_{k,m} \mathbf{w}_{k,m}}{\|\mathbf{w}_{k,m}\|^2} \\ &= \max_{\mathbf{w}_{k,m} \in \mathcal{W}_{k,m}^d} \frac{\mathbf{w}_{k,m}^H \Xi_{k,m}^d \mathbf{w}_{k,m}}{\|\mathbf{w}_{k,m}\|^2} \leq \lambda_{\max}(\Xi_{k,m}^d). \end{aligned} \quad (60)$$

In the above derivations, the first equality follows from (25), (29), and (45); the second equality is a consequence of the fact that $(\mathbf{I}_T \otimes \mathbf{\Pi}_{k,m}^d) \mathbf{w}_{k,m} = \mathbf{w}_{k,m}$ if $\mathbf{w}_{k,m} \in \mathcal{W}_{k,m}^d$; finally, the last inequality is tight when $\mathbf{w}_{k,m}$ is proportional to the eigenvector corresponding to the largest eigenvalue of $\Xi_{k,m}^d$. The result for $\kappa_{k,m} = 0$ follows by similar arguments.

D. Proof of Proposition 5

Upon solving for the optimal $\mathbf{w}_{k,m}$ as reported in Proposition 4, the constraint C3 can be reformulated as

$$\begin{cases} \lambda_{\max}(\Xi_{k,m}^d) \geq \rho_{k,m}^d, & \text{if } \kappa_{k,m} = \infty, \\ \lambda_{\max}(\Xi_{k,m}^i) \geq \rho_{k,m}^i, & \text{if } \kappa_{k,m} = 0, \end{cases} \quad \forall k, m. \quad (61)$$

If $\kappa_{k,m} = \infty$, then we have

$$\begin{aligned} \lambda_{\max}(\Xi_{k,m}^d) &= \frac{|\beta_{k,m,0}|^2}{\sigma_{z,k,m}^2} \left\| (\mathbf{I}_T \otimes \mathbf{\Pi}_{k,m}^d) \right. \\ &\quad \times \left. (\mathbf{I}_T \otimes \mathbf{g}_{k,m}(\bar{\phi}_{m,0}) \mathbf{s}_k^T(\phi_{m,0})) \mathbf{u}_k \right\|^2 \\ &= \frac{|\beta_{k,m,0}|^2}{\sigma_{z,k,m}^2} \mathbf{g}_{k,m}^H(\bar{\phi}_{m,0}) \mathbf{\Pi}_{k,m}^d \mathbf{g}_{k,m}(\bar{\phi}_{m,0}) \\ &\quad \times \mathbf{u}_k^H (\mathbf{I}_T \otimes \mathbf{s}_k^*(\phi_{m,0}) \mathbf{s}_k^T(\phi_{m,0})) \mathbf{u}_k \\ &= \frac{|\beta_{k,m,0}|^2}{\sigma_{z,k,m}^2} \mathbf{g}_{k,m}^H(\bar{\phi}_{m,0}) \mathbf{\Pi}_{k,m}^d \mathbf{g}_{k,m}(\bar{\phi}_{m,0}) \\ &\quad \times \text{Tr}\{\mathbf{U}_k^H \mathbf{s}_k^*(\phi_{m,0}) \mathbf{s}_k^T(\phi_{m,0}) \mathbf{U}_k\}. \end{aligned} \quad (62)$$

The above derivations show that we must necessarily have $\mathbf{U}_k^H \mathbf{s}_k^*(\phi_{m,0}) \neq \mathbf{0}_{N_t}$, as otherwise $\lambda_{\max}(\Xi_{k,m}) = 0$. Also, if $\text{rank}\{\mathbf{U}_k\} = N_t$, we can write [64]

$$\begin{aligned} \lambda_{\max}(\Xi_{k,m}^d) &\geq \frac{N_t |\beta_{k,m,0}|^2}{\sigma_{z,k,m}^2} \lambda_{\min}(\mathbf{U}_k \mathbf{U}_k^H) \\ &\quad \times \mathbf{g}_{k,m}^H(\bar{\phi}_{m,0}) \mathbf{\Pi}_{k,m}^d \mathbf{g}_{k,m}(\bar{\phi}_{m,0}) \end{aligned} \quad (63)$$

and C3 can be satisfied if (46) holds.

If $\kappa_{k,m} = 0$, from the Weyl's Theorem [64] we have

$$\begin{aligned} \lambda_{\max}(\Xi_{k,m}^i) &\leq \sum_{q=1}^{Q_m} \frac{\sigma_{\beta,k,m,q}^2}{\sigma_{z,k,m}^2} \mathbf{g}_{k,m}^H(\bar{\phi}_{m,q}) \mathbf{\Pi}_{k,m}^i \mathbf{g}_{k,m}(\bar{\phi}_{m,q}) \\ &\quad \times \text{Tr}\{\mathbf{U}_k^H \mathbf{s}_k^*(\phi_{m,q}) \mathbf{s}_k^T(\phi_{m,q}) \mathbf{U}_k\} \end{aligned} \quad (64a)$$

$$\begin{aligned} \lambda_{\max}(\Xi_{k,m}^i) &\geq \max_q \frac{\sigma_{\beta,k,m,q}^2}{\sigma_{z,k,m}^2} \mathbf{g}_{k,m}^H(\bar{\phi}_{m,q}) \mathbf{\Pi}_{k,m}^i \mathbf{g}_{k,m}(\bar{\phi}_{m,q}) \\ &\quad \times \text{Tr}\{\mathbf{U}_k^H \mathbf{s}_k^*(\phi_{m,q}) \mathbf{s}_k^T(\phi_{m,q}) \mathbf{U}_k\}. \end{aligned} \quad (64b)$$

The above inequalities show that we must necessarily have $\mathbf{U}_k^H \mathbf{s}_k^*(\phi_{m,q}) \neq \mathbf{0}_{N_t}$ for at least one indirect path $q \in \{1, \dots, Q_m\}$. Also, if $\text{rank}\{\mathbf{U}_k\} = N_t$, we can write [64]

$$\begin{aligned} \lambda_{\max}(\Xi_{k,m}^i) &\geq \max_q \frac{N_t \sigma_{\beta,k,m,q}^2}{\sigma_{z,k,m}^2} \lambda_{\min}(\mathbf{U}_k \mathbf{U}_k^H) \\ &\quad \times \mathbf{g}_{k,m}^H(\bar{\phi}_{m,q}) \mathbf{\Pi}_{k,m}^i \mathbf{g}_{k,m}(\bar{\phi}_{m,q}) \end{aligned} \quad (65)$$

and C3 can be satisfied if (46) holds.

REFERENCES

- [1] H. Griffiths *et al.*, "Radar spectrum engineering and management: Technical and regulatory issues," *Proceedings of the IEEE*, vol. 103, no. 1, pp. 85–102, Jan. 2015.
- [2] H. Mazar, *Radio spectrum Management: Policies, regulations and techniques*. USA: John Wiley & Sons, 2016.
- [3] N. Devroye, M. Vu, and V. Tarokh, "Cognitive radio networks," *IEEE Signal Processing Magazine*, vol. 25, no. 6, pp. 12–23, Nov. 2008.
- [4] J. Proakis and M. Salehi, *Digital Communications*, 5th ed. New York, NY, USA: McGraw-Hill Higher Education, 2014.
- [5] L. Dai *et al.*, "A survey of non-orthogonal multiple access for 5G," *IEEE Communications Surveys Tutorials*, vol. 20, no. 3, pp. 2294–2323, thirdquarter 2018.

- [6] L. Venturino, N. Prasad, and X. Wang, "Coordinated scheduling and power allocation in downlink multicell OFDMA networks," *IEEE Transactions on Vehicular Technology*, vol. 58, no. 6, pp. 2835–2848, Jul. 2009.
- [7] H. Zhang *et al.*, "Weighted sum-rate maximization in multi-cell networks via coordinated scheduling and discrete power control," *IEEE Journal on Selected Areas in Communications*, vol. 29, no. 6, pp. 1214–1224, Jun. 2011.
- [8] E. Björnson and L. Sanguinetti, "Scalable cell-free massive MIMO systems," *IEEE Transactions on Communications*, vol. 68, no. 7, pp. 4247–4261, Jul. 2020.
- [9] L. Venturino, N. Prasad, X. Wang, and M. Madhian, "Design of linear dispersion codes for practical MIMO-OFDM systems," *IEEE Journal of Selected Topics in Signal Processing*, vol. 1, no. 1, pp. 178–188, Jun. 2007.
- [10] N. Fatema, G. Hua, Y. Xiang, D. Peng, and I. Natgunanathan, "Massive MIMO linear precoding: A survey," *IEEE Systems Journal*, vol. 12, no. 4, pp. 3920–3931, Dec. 2018.
- [11] M. A. Albreem, M. Juntti, and S. Shahabuddin, "Massive MIMO detection techniques: A survey," *IEEE Communications Surveys Tutorials*, vol. 21, no. 4, pp. 3109–3132, Fourthquarter 2019.
- [12] S. H. Javadi and A. Farina, "Radar networks: A review of features and challenges," *Information Fusion*, vol. 61, pp. 48–55, 2020.
- [13] S. Miranda, C. Baker, K. Woodbridge, and H. Griffiths, "Knowledge-based resource management for multifunction radar: a look at scheduling and task prioritization," *IEEE Signal Processing Magazine*, vol. 23, no. 1, pp. 66–76, Jan. 2006.
- [14] S. Z. Gurbuz *et al.*, "An overview of cognitive radar: Past, present, and future," *IEEE Aerospace and Electronic Systems Magazine*, vol. 34, no. 12, pp. 6–18, Dec. 2019.
- [15] J. Li and P. Stoica, *MIMO radar signal processing*. Hoboken, USA: John Wiley & Sons, 2009.
- [16] S. D. Blunt and E. L. Mokole, "Overview of radar waveform diversity," *IEEE Aerospace and Electronic Systems Magazine*, vol. 31, no. 11, pp. 2–42, Nov. 2016.
- [17] E. Grossi, M. Lops, and L. Venturino, "Robust waveform design for MIMO radars," *IEEE Transactions on Signal Processing*, vol. 59, no. 7, pp. 3262–3271, Jul. 2011.
- [18] E. Grossi, M. Lops, and L. Venturino, "Min–max waveform design for MIMO radars under unknown correlation of the target scattering," *Signal Processing*, vol. 92, no. 6, pp. 1550–1558, 2012.
- [19] W. Roberts, P. Stoica, J. Li, T. Yardibi, and F. A. Sadjadi, "Iterative adaptive approaches to MIMO radar imaging," *IEEE Journal of Selected Topics in Signal Processing*, vol. 4, no. 1, pp. 5–20, Feb 2010.
- [20] J. Liu and J. Li, "Robust detection in MIMO radar with steering vector mismatches," *IEEE Transactions on Signal Processing*, vol. 67, no. 20, pp. 5270–5280, Oct. 2019.
- [21] K. Alhujaili, V. Monga, and M. Rangaswamy, "Transmit MIMO radar beampattern design via optimization on the complex circle manifold," *IEEE Transactions on Signal Processing*, vol. 67, no. 13, pp. 3561–3575, Jul. 2019.
- [22] X. Yu, G. Cui, J. Yang, L. Kong, and J. Li, "Wideband MIMO radar waveform design," *IEEE Transactions on Signal Processing*, vol. 67, no. 13, pp. 3487–3501, Jul. 2019.
- [23] L. Zheng, M. Lops, Y. C. Eldar, and X. Wang, "Radar and communication coexistence: An overview: A review of recent methods," *IEEE Signal Processing Magazine*, vol. 36, no. 5, pp. 85–99, Sep. 2019.
- [24] F. Liu, C. Masouros, A. Petropulu, H. Griffiths, and L. Hanzo, "Joint radar and communication design: Applications, state-of-the-art, and the road ahead," *IEEE Transactions on Communications*, vol. 68, no. 6, pp. 3834 – 3862, Jun. 2020.
- [25] N. C. Luong, X. Lu, D. T. Hoang, D. Niyato, and D. I. Kim, "Radio resource management in joint radar and communication: A comprehensive survey," *IEEE Communications Surveys Tutorials*, vol. 23, no. 2, pp. 780–814, 2021.
- [26] F. Wang, H. Li, and M. A. Govoni, "Power allocation and co-design of multicarrier communication and radar systems for spectral coexistence," *IEEE Transactions on Signal Processing*, vol. 67, no. 14, pp. 3818–3831, Jul. 2019.
- [27] Z. Cheng, B. Liao, S. Shi, Z. He, and J. Li, "Co-design for overlaid MIMO radar and downlink MISO communication systems via Cramér–Rao bound minimization," *IEEE Transactions on Signal Processing*, vol. 67, no. 24, pp. 6227–6240, Dec. 2019.
- [28] E. Grossi, M. Lops, and L. Venturino, "Joint design of surveillance radar and MIMO communication in cluttered environments," *IEEE Transactions on Signal Processing*, vol. 68, pp. 1544–1557, 2020.
- [29] E. Grossi, M. Lops, and L. Venturino, "Energy efficiency optimization in radar-communication spectrum sharing," *IEEE Transactions on Signal Processing*, vol. 69, pp. 3541–3554, 2021.
- [30] J. Qian, L. Venturino, M. Lops, and X. Wang, "Radar and communication spectral coexistence in range-dependent interference," *IEEE Transactions on Signal Processing*, vol. 69, pp. 5891–5906, 2021.
- [31] E. Grossi, M. Lops, and L. Venturino, "Adaptive detection and localization exploiting the IEEE 802.11ad standard," *IEEE Transactions on Wireless Communications*, vol. 19, no. 7, pp. 4394–4407, Jul. 2020.
- [32] E. Grossi, M. Lops, A. M. Tulino, and L. Venturino, "Opportunistic sensing using mmwave communication signals: A subspace approach," *IEEE Transactions on Wireless Communications*, vol. 20, no. 7, pp. 4420–4434, Jul 2021.
- [33] A. Hassanien, M. G. Amin, Y. D. Zhang, and F. Ahmad, "Signaling strategies for dual-function radar communications: an overview," *IEEE Aerospace and Electronic Systems Magazine*, vol. 31, no. 10, pp. 36–45, Oct. 2016.
- [34] A. Ahmed, Y. D. Zhang, and Y. Gu, "Dual-function radar-communications using QAM-based sidelobe modulation," *Digital Signal Processing*, vol. 82, pp. 166–174, 2018.
- [35] T. Huang, N. Shlezinger, X. Xu, Y. Liu, and Y. C. Eldar, "MAJoRCom: A dual-function radar communication system using index modulation," *IEEE Transactions on Signal Processing*, vol. 68, pp. 3423–3438, 2020.
- [36] C. Sturm and W. Wiesbeck, "Waveform design and signal processing aspects for fusion of wireless communications and radar sensing," *Proceedings of the IEEE*, vol. 99, no. 7, pp. 1236–1259, Jul. 2011.
- [37] D. Ma, N. Shlezinger, T. Huang, Y. Liu, and Y. C. Eldar, "Joint radar-communication strategies for autonomous vehicles: Combining two key automotive technologies," *IEEE Signal Processing Magazine*, vol. 37, no. 4, pp. 85–97, Jul. 2020.
- [38] M. Bicá and V. Koivunen, "Generalized multicarrier radar: Models and performance," *IEEE Transactions on Signal Processing*, vol. 64, no. 17, pp. 4389–4402, Sep. 2016.
- [39] A. Ahmed, Y. D. Zhang, A. Hassanien, and B. Himed, "OFDM-based joint radar-communication system: Optimal sub-carrier allocation and power distribution by exploiting mutual information," in *2019 53rd Asilomar Conference on Signals, Systems, and Computers*, Nov. 2019, pp. 559–563.
- [40] C. Shi, Y. Wang, F. Wang, S. Salous, and J. Zhou, "Joint optimization scheme for subcarrier selection and power allocation in multicarrier dual-function radar-communication system," *IEEE Systems Journal*, vol. 15, no. 1, pp. 947–958, Mar. 2021.
- [41] M. Bicá and V. Koivunen, "Multicarrier radar-communications waveform design for RF convergence and coexistence," in *ICASSP 2019 - 2019 IEEE International Conference on Acoustics, Speech and Signal Processing (ICASSP)*, May 2019, pp. 7780–7784.
- [42] M. Temiz, E. Alsusa, and M. W. Baidas, "A dual-functional massive MIMO OFDM communication and radar transmitter architecture," *IEEE Transactions on Vehicular Technology*, vol. 69, no. 12, pp. 14974–14988, Dec. 2020.
- [43] M. Temiz, E. Alsusa, and M. W. Baidas, "Optimized precoders for massive MIMO OFDM dual radar-communication systems," *IEEE Transactions on Communications*, vol. 69, no. 7, pp. 4781–4794, Jul. 2021.
- [44] M. Temiz, E. Alsusa, and M. W. Baidas, "A dual-function massive MIMO uplink OFDM communication and radar architecture," *IEEE Transactions on Cognitive Communications and Networking*, 2021.
- [45] G. H. Hardy, J. E. Littlewood, and G. Pólya, *Inequalities*. Cambridge, UK: Cambridge University Press, 1934.
- [46] P. Bullen, *Handbook of Means and Their Inequalities*, ser. Mathematics and Its Applications. Netherlands: Springer, 2003.
- [47] H. Lee and S. Kim, "Muirhead's and Holland's inequalities of mixed power means for positive real numbers," *Journal of applied mathematics & informatics*, vol. 35, no. 1–2, p. 33–44, Jan. 2017.
- [48] Y. Yang and R. S. Blum, "MIMO radar waveform design based on mutual information and minimum mean-square error estimation," *IEEE Transactions on Aerospace and Electronic Systems*, vol. 43, no. 1, pp. 330–343, Jan. 2007.
- [49] A. De Maio, M. Lops, and L. Venturino, "Diversity-integration tradeoffs in MIMO detection," *IEEE Transactions on Signal Processing*, vol. 56, no. 10, pp. 5051–5061, Oct. 2008.
- [50] S. Sen and A. Nehorai, "OFDM MIMO radar with mutual-information waveform design for low-grazing angle tracking," *IEEE Transactions on Signal Processing*, vol. 58, no. 6, pp. 3152–3162, Jun. 2010.
- [51] A. Aubry, M. Lops, A. M. Tulino, and L. Venturino, "On MIMO detection under non-Gaussian target scattering," *IEEE Transactions on Information Theory*, vol. 56, no. 11, pp. 5822–5838, Nov. 2010.

- [52] G. H. Jajamovich, M. Lops, and X. Wang, "Space-time coding for MIMO radar detection and ranging," *IEEE Transactions on Signal Processing*, vol. 58, no. 12, pp. 6195–6206, Dec. 2010.
- [53] M. A. Richards, *Fundamentals of radar signal processing*. New York, NY, USA: McGraw-Hill, 2005.
- [54] E. Grossi and M. Lops, "Space-time code design for MIMO detection based on Kullback-Leibler divergence," *IEEE Transactions on Information Theory*, vol. 58, no. 6, pp. 3989–4004, 2012.
- [55] M. I. Skolnik, *Introduction to radar systems*, 3rd ed., ser. McGraw-Hill international editions. Electrical engineering series. Boston, MA, USA: McGraw-Hill, 2001.
- [56] J. A. Roberts and J. M. Bargallo, "DPSK performance for indoor wireless Rician fading channels," *IEEE Transactions on Communications*, vol. 42, no. 234, pp. 592–596, 1994.
- [57] S. Jonqyin and I. S. Reed, "Performance of MDPSK, MPSK, and non-coherent MFSK in wireless Rician fading channels," *IEEE Transactions on Communications*, vol. 47, no. 6, pp. 813–816, Jun. 1999.
- [58] K. Lange, "A tutorial on MM algorithms," *The American Statistician*, vol. 58, no. 1, p. 30–37, Feb. 2004.
- [59] B. C. Rennie, "Exponential means," *James Cook Mathematical Notes*, vol. 6, no. 54, pp. 6023–6024, Feb. 1991.
- [60] C. K. Pauw and D. L. Schilling, "Probability of error of M -ary PSK and DPSK on a Rayleigh fading channel," *IEEE Transactions on Communications*, vol. 36, no. 6, pp. 755–756, 1988.
- [61] S. Boyd, S. P. Boyd, and L. Vandenberghe, *Convex optimization*. Cambridge, United Kingdom: Cambridge University Press, 2004.
- [62] A. B. Gershman, Z.-Q. Luo, and S. Shahbazpanahi, "Robust adaptive beamforming based on worst-case performance optimization," in *Robust Adaptive Beamforming*, Ian Li and P. Stoica, Eds. Hoboken, New Jersey: John Wiley & Sons, 2006, ch. 2, pp. 49–89.
- [63] N. Sidiropoulos, T. Davidson, and Z.-Q. Luo, "Transmit beamforming for physical-layer multicasting," *IEEE Transactions on Signal Processing*, vol. 54, no. 6, pp. 2239–2251, 2006.
- [64] R. A. Horn and C. R. Johnson, *Matrix Analysis*, 2nd ed. USA: Cambridge University Press, 2012.